A Mesenchymal Cell Niche in Skin for Acute Myeloid Leukemia

Running title: Extramedullary mesenchymal cell niche in AML

Lakshmi Sandhow[1], Huan Cai[1], Pingnan Xiao[1], Elory Leonard[1], Makoto Kondo[1&], Xiaoyan Sun[2], Anne-Sofie Johansson[1], Karl Tryggvason[3], Maria Kasper[2], Marcus Järås[4], Hong Qian[1*]

[1]Center for Hematology and Regenerative Medicine, Department of Medicine Huddinge, Karolinska Institute, Karolinska University Hospital, SE-141 86 Stockholm, Sweden;

[2]Department of Cell and Molecular Biology, Karolinska Institute, 171 77, Stockholm, Sweden;

[3]Department of Medical Biochemistry and Biophysics, Karolinska Institute, Stockholm, 17177, Sweden;

[4]Department of Clinical Genetics, Lund University, Lund 22184, Sweden.

[&]Current address: Cell Sheet Tissue Engineering Center (CSTEC), Department of Pharmaceutics and Pharmaceutical Chemistry, Health Sciences, University of Utah, 30 South 2000 East, Salt Lake City, Utah 84112, USA.

***Corresponding author:** Hong Qian, hong.qian@ki.se

Text word count: 3993 excluding acknowledgments
Abstract word count: 149
Figures: 7 main figures, 6 supplemental figures
References: 61

Key points:

- Leukemic cells infiltrated in skin are capable to generate AML post-transplantation
- Mesenchymal progenitors in skin contribute to forming the niche for AML cells
- Skin mesenchymal progenitors protect AML stem cells possibly by mitochondrial transfer
- *Lama4* deletion in skin mesenchymal niche promotes AML cell proliferation and chemoresistance to cytarabine

Abstract (149)

Leukemia cutis or leukemic cell infiltration in skin is one of the common extramedullary manifestations of acute myeloid leukemia (AML) and signifies a poorer prognosis. However, its pathogenesis and maintenance remain understudied. Here, we report massive AML cell infiltration in mouse skin. These cells were retained in the skin post-chemotherapy and could regenerate AML post-transplantation. The niche characterization revealed that skin harbored mesenchymal progenitor cells (MPCs) with a similar phenotype as BM mesenchymal stem cells. These skin MPCs maintained and protected AML-initiating stem cells (LSCs) from chemotherapy *in vitro* possibly via mitochondrial transfer. Furthermore, *Lama4* deletion in skin MPCs promoted AML LSC proliferation and chemoresistance. Importantly, more chemoresistant AML LSCs were retained in *Lama4*$^{-/-}$ mouse skin post-cytarabine treatment. Our study reveals the characteristics and previously unrecognized roles of skin mesenchymal niches in maintaining AML LSCs and protecting them during chemotherapy, meriting future exploration of their impact on AML relapse.

Key words: Early B-cell Factor 2, skin, mesenchymal progenitor cells, acute myeloid leukemia, hematopoietic stem cells, stem cell niche, leukemic stem cells, drug resistance, cytarabine, bone marrow

Introduction

Leukemia cutis (leukemic cell infiltration in skin) is one of the commonly observed extramedullary manifestations in acute myeloid leukemia (AML).[1,2] It is associated with poor survival in patients with AML.[2-4] However, our understanding of its pathogenesis is very limited. This has been mainly due to lack of knowledge about the extramedullary niches where AML cells infiltrate and are maintained.

For decades, great efforts have been put to elucidate the contribution of the hematopoietic niche in bone marrow (BM) to normal and malignant hematopoiesis. The BM niche consists of various types of cells including mesenchymal stem cells (MSCs), mesenchymal progenitors (MPCs), osteoblasts and endothelial cells. Accumulating evidence has shown that BM MSCs and MPCs play important roles in maintaining normal hematopoiesis and in the development of myeloid malignancies including AML.[5,6] Molecular alterations in these niches could lead to malignant transformation of hematopoietic cells.[7-9] During leukemia development, the leukemic cells can alter the BM niches, which renders the niche to become favorable for

leukemic cell growth but harmful for normal hematopoiesis.[6,10-13] Using a *Cre-LoxP* mouse model allowing for selective deletion of the MSC population, we have shown that loss of MSCs accelerates AML progression.[6,10] However, these markers are not unique for the mesenchymal cells in BM, thus, it is not clear whether the mesenchymal cell niches in extramedullary organs like skin are also affected, thereby contributing to the AML progression.

Besides BM, extramedullary organs such as adipose tissue have been reported to accommodate hematopoietic stem and progenitor cells (HSPCs) in the stromal vascular fraction.[14] In blast crisis of chronic myeloid leukemia, the gonadal white adipose tissue is infiltrated by leukemic cells that adapt to the extramedullary niche and transform into resistant leukemia-initiating stem cells (LSCs) marked by CD36 expression.[15] These findings indicate that extramedullary organs may serve as niches for HSPCs and LSCs.

Existing evidence suggests that skin might contain an MSC-like cell population.[16-19] However, their biological properties and contribution to hematopoiesis and leukemia remain unexplored. Knowledge of this would be essential for understanding the pathology of extramedullary leukemia in the skin, and would thus provide new insights into identifying new potential therapeutic targets that may be translated into new treatment strategies for AML patients with leukemia cutis.

We here in a transplantation-induced AML mouse model detected massive infiltration of AML cells in the skin. Importantly, these skin AML cells from mice at steady-state or post-chemotherapy could regenerate AML post-secondary transplantation. Characterization of the AML niche revealed the molecular features and developmental hierarchy of the skin MPCs. The MPCs expressing Early B-cell Factor 2 (Ebf2) contribute to mesenchymal cell turnover in the skin and were reduced post-AML onset. The skin MPCs could maintain and protect AML LSCs and loss of Lama4 in skin MPCs promoted AML cell maintenance and resistance to chemotherapy. Altogether, our study revealed the characteristics and a previously unrecognized role of skin MPCs in maintaining AML LSCs during AML development and chemotherapy.

Results

The AML cells infiltrated in skin can regenerate AML post-transplantation

We have here studied extramedullary leukemia in skin by using an MLL-AF9^{+} AML cell transplantation-induced AML mouse model (**Figure 1A**). Post-symptomatic AML onset, we detected the massive infiltration of the AML cells in the dorsal skin by fluorescence-activated

cell sorting (FACS) (**Figure 1B-1D**). The frequency was higher (41% of skin CD45$^+$ cells) than that in the blood, but lower than that in BM (>95%) (**Figure 1B-1C**). Confocal imaging showed that these AML cells mainly resided at perivascular sites in the skin (**Figure 1D**).

It is not known whether the AML cells infiltrated in skin contain LSCs capable to regenerate leukemia, particularly after chemotherapy. We therefore sorted the AML cells from the mouse skin post-cytarabine (Ara-C) or vehicle treatment and transplanted them into secondary recipients without prior irradiation (**Figure 1E-1K**). Notably, these AML cells even in a low dose (1000 cells/mouse) rapidly and efficiently generated AML in the recipients without pre-conditioning, as indicated by short survival (**Figure 1F**), low platelet counts (**Figure 1G**), high AML engraftment in the BM (**Figure 1H-1I)** and splenomegaly (**Figure 1J**). These results demonstrate the leukemia-initiating capacity of the AML cells residing in the skin tissue not only under steady-state but also after chemotherapy, indicating their potential impact in AML relapse.

Skin harbors Ebf2$^+$ and Ebf2$^-$ MPC subsets with similar immunophenotype to BM MSCs

To understand how the leukemic cells were maintained in the skin tissue, we explored the role of the extramedullary microenvironment in the skin using a similar approach as was used for characterizing the BM niche. BM MSCs have been shown to be involved in AML progression in mice[6]. They are defined by a phenotype of lacking expression of CD44, hematopoietic (CD45/TER119) and endothelial (CD31) cell markers, but positive for PDGFRa/CD140a, SCA1 and CD51.[6,9,11,20,21] The primitive MSCs in mouse BM can be identified by Ebf2 expression[22] and can generate MSCs that lack Ebf2.[6] However, the phenotype of native skin MSCs remains unknown. The question is whether the cells with similar features exist in skin and play a role in the AML cell maintenance under steady-state and following chemotherapy. To answer this, we first characterized mesenchymal stem and progenitors in the skin by using the *Ebf2-Egfp* reporter mice. Similar to BM, a fraction of CD45$^-$TER119$^-$CD31$^-$ skin stromal cells expressed Ebf2 (**Figure 2A**). The Ebf2$^+$ cells accounted for about 2% and 5% of total live cells and CD45$^-$TER119$^-$CD31$^-$ stromal cells, respectively (**Figure 2B-2C**). Phenotypically, skin Ebf2$^+$ cells highly expressed PDGFRa/CD140a and SCA1 (PαS) whereas about 41% of the Ebf2$^-$ cells were PαS cells (**Figure 2D**).

Functionally, both the Ebf2$^+$ and Ebf2$^-$ cells contained CFU-Fs, a colony-forming unit characteristic for MSCs (**Figure 2E, Figure S1A**). The CFU-Fs in the Ebf2$^+$ cells were

generated exclusively by the SCA1$^+$ population (**Figure 2F**). Both Ebf2$^+$ and Ebf2$^-$PαS cell populations showed similar proliferation kinetics after passage 5-6 (**Figure S1B**) and were able to differentiate towards osteogenic and adipogenic lineages *in vitro* (**Figure S1C**). However, they failed to differentiate into chondrocytes in either monolayer or micromass pellet culture in which condition BM MSCs could differentiate into chondrocytes (**Figure S1C-S1D**). These data indicate that the Ebf2$^+$ and Ebf2$^-$PαS cells in mouse skin may represent bipotential MPCs although they have the same immunophenotype as BM MSCs.

Single-cell assay confirms osteo-adipo bipotentials of skin Ebf2$^+$ and Ebf2$^-$PαS cells

To validate the identity of the skin stromal subsets, we characterized these cells at single cell level. Limiting dilution experiment revealed that the CFU-F frequency in both skin Ebf2$^+$ and Ebf2$^-$PαS fractions was as high as 1 in 4 (**Figure 2G, 2I**). Of 8 randomly selected CFU-Fs from single Ebf2$^+$ cells, 7 (88%) showed both osteogenic and adipogenic differentiation potency although to different degrees (**Figure 2H, 2K**). However, only 43% (3 clones of 7) of the Ebf2$^-$PαS cells showed bi-lineage potency toward osteoblasts and adipocytes (**Figure 2J-2K**). The chondrogenic potency, however, was not evaluated at single cell level since none of these cell subsets differentiated into chondrocytes at the bulk level. The self-renewal capacity of the Ebf2$^+$ and Ebf2$^-$ cells was evaluated by serially replating of single CFU-F derived from the single sorted cells. Three out of 5 clones from 12 CFU-Fs initially generated by single Ebf2$^+$ cells could be serially replated for beyond 10 passages while the other 2 clones were able to expand to passage 5 (**Figure 2L**). Meanwhile, only 1 in 3 CFU-F clones derived from 9 Ebf2$^-$PαS cells-derived CFU-Fs could be serially replated for over 8 passages (**Figure 2L**), indicating a limited self-renewal capacity of the Ebf2$^-$PαS cells. These data further support the notion that the skin Ebf2$^+$ and Ebf2$^-$PαS cells are enriched with osteo-adipogenic MPCs.

Skin Ebf2$^+$ cells are mainly located at perivascular sites

Similar to that in mouse BM, the skin Ebf2$^+$ cells did not express endothelial cell marker CD31 (**Figure S2A**). However, the Ebf2$^+$ cells highly expressed PDGFRb/CD140b, a marker expressed in pericytes[23] and niche-forming perivascular cells in BM[24] (**Figure S2B**), pointing to a pericyte phenotype. Confocal imaging illustrated that the majority of the Ebf2$^+$ cells were adjacent to the endothelial cells in the skin (**Figure 3A-3B**, **Figure S2C**). Some scattered Ebf2$^+$ cells were also found in dermal panniculus carnosus, a layer of striated muscle (**Figure 3A**). Approximately 55% and 41% of the Ebf2$^+$ cells were positive for the pericyte marker NG2,

respectively (**Figure S2D, S2F**), and 81% of them expressed α-smooth muscle actin (SMA) (**Figure S2E-S2F**), reported to mark pericytes in BM[25]. Altogether, these data suggest a perivascular origin and heterogeneity of the skin Ebf2$^+$ cells.

The Ebf2$^+$ cells in skin contribute to the mesenchymal cell turnover

To understand how mesenchymal cell niche in the skin is maintained, we determined the physiological contribution of the Ebf2$^+$ stromal cells to the niche formation by lineage-tracing using Tg*Ebf2-Egfp xCre^{ERT2}* X *Rosa26-tomato* mice (**Figure 3C**). This mouse model allowed us to track the fates of the Ebf2$^+$ cells *in vivo* since the Ebf2$^+$ cells express GFP and their progeny is marked by Tomato after tamoxifen (TAM) injection. About 15% of total Ebf2$^+$ cells were Tomato$^+$(Ebf2$^+$Tomato$^+$) cells at 3 months after TAM induction (**Figure S3A-S3B**). The Ebf2$^+$Tomato$^+$ cells could generate Ebf2$^-$PαS MPCs and more mature CD45$^-$TER119$^-$CD31$^-$ CD44$^-$CD140a$^+$SCA1$^-$ stromal cells (**Figure 3D-3E**), indicating the important role of the Ebf2$^+$ cells in maintaining the mesenchymal cell compartment in the skin.

The fraction of the Ebf2$^+$Tomato$^+$ cells within stromal cells remained constant up to 12 months post TAM induction (**Figure 3E**), which is likely attributed to their self-renewal ability. However, the Ebf2$^-$Tomato$^+$ cells which were produced by the Ebf2$^+$Tomato$^+$ cells increased from 11% at 3 months to 21% at 6 months post-TAM injection, then remained stable at 12 months (**Figure 3E**). Within the newly generated Ebf2$^-$Tomato$^+$ cells, the majority were PαS MPCs and about 5% were the CD140a$^+$SCA1$^-$ cells (**Figure 3F**). Within the total PαS MPCs, only about 0.5% were Ebf2$^+$Tomato$^+$ cells and 30% were the newly generated Ebf2$^-$Tomato$^+$) PαS cells at 6 months post-TAM (**Figure S3C-S3E**). These data suggest a substantial contribution of the Ebf2$^+$ MPCs to generating the Ebf2$^-$Tomato$^+$PαS MPCs while maintaining the Ebf2$^+$ cell pool. The actual contribution might have been underestimated due to the incomplete *Cre* activation in the Ebf2$^+$ cells, reflected in the presence of Ebf2$^+$Tomato$^-$ cells shortly (2-3days) after TAM injection (data now shown).

Similar to the Ebf2$^+$ cells, the Ebf2$^-$Tomato$^+$ cells were mainly distributed in the lower dermis and adjacent to CD31$^+$ endothelial cells (**Figure 3G**). Unlike the Ebf2$^+$ cells, the Ebf2$^-$ Tomato$^+$ cells lacked NG2 expression (**Figure S3F**). Only 19% and 28% of the Ebf2$^-$Tomato$^+$ cells expressed NESTIN and α-SMA, respectively (**Figure S3G-SI**),

Altogether, skin harbors Ebf2$^+$ and Ebf2$^-$PαS MPCs with a similar phenotype as BM MSCs. The Ebf2$^+$ MPCs reside at the top of the developmental hierarchy and contribute to mesenchymal cell generation in the skin.

197

198 **Skin MPCs play a role in maintaining normal hematopoietic and AML cells *in vitro***

199 Identification of the skin MPC populations made it possible to analyze their potential role
200 in the maintenance of AML cells. We first evaluated the function of skin MPC subsets in
201 supporting normal hematopoietic stem cells (HSCs) in a co-culture system and compared to
202 BM MSCs (**Figure S4A**). Similar to their BM counterparts, both skin Ebf2^{+} and Ebf2^{-}PαS
203 MPCs were able to maintain HSC activities**,** indicated by similar numbers of CFU-Cs generated
204 from the SCA1^{+}KIT^{+}(LSK)CD150^{+} cells after the co-coculture with skin MPCs or BM MSCs
205 (**Figure S4B-S4C**). This finding was further supported by the similar cobblestone area forming
206 cells (CAFCs) generated from the BM LSK cells co-cultured with the skin MPCs or BM MSCs
207 (**Figure S4D-S4E**). The BM Ebf2^{-}PαS cells displayed better capacity in supporting CAFC
208 formation from the LSK cells than the BM Ebf2^{+} MSCs (**Figure S4F**). Altogether, these data
209 indicated that skin MPCs possessed similar hematopoiesis supportive function as BM MSCs.
210 To assess the role of skin MPCs in supporting AML LSC growth, we next performed CAFC
211 assay of MLL-AF9^{+} AML cells (**Figure 4A**). Like BM Ebf2^{+} MSCs, skin MPC subsets could
212 support CAFC formation from the AML cells, but to a lesser degree than the BM Ebf2^{-}PαS
213 cells (**Figure 4B-4C**).
214 Increasing evidence suggests that BM stromal cells may protect leukemia cells from
215 cytostatic drugs.[26-30] However, it is not known if extramedullary stromal cells have similar
216 functions. We then tested the chemoprotective function of skin MPCs by CAFC assay. We
217 administered Ara-C 2 days after seeding the MLL-AF9^{+} AML cells to the MPCs to allow for
218 efficient cell-cell interactions (**Figure 4A**). Both skin Ebf2^{+} and Ebf2^{-}PαS cells could protect
219 the AML LSCs from Ara-C treatment, demonstrated by the persistence of residual CAFCs after
220 Ara-C treatment, in striking contrast to the efficient killing of the AML cells cultured alone
221 (**Figure 4D-4E**). No difference in the frequency of KIT^{+} AML cells, representing AML
222 LSCs,[31] was observed among all the co-cultures (**Figure 4F**). However, the numbers of the
223 residual KIT^{+} LSCs were significantly increased in the co-cultures with the stromal cells
224 compared to the monoculture post-Ara-C treatment (**Figure 4G**). CD36 was reported to be a
225 marker for chemoresistant leukemic cells.[15,32,33] Post-Ara-C, the CD36^{+} AML cells were
226 selectively enriched in all the co-cultures except that with skin Ebf2^{-}PαS MPCs (**Figure 4H**),
227 however, only in the culture with skin MPC subsets, significant more CD36^{+} AML cells were
228 retained (**Figure 4I**). These data indicate a previously unrecognized role of skin MPCs in AML
229 LSC maintenance and protection.

The altered mesenchymal niches in the skin during AML development.

Niche-remodeling in BM has been considered as one of the mechanisms contributing to leukemia progression[6,34-36]. By confocal imaging, we observed the perivascular location of the AML cells (**Figure 1D**) and the localization adjacent to the skin Ebf2/GFP$^+$ MPCs in the skin (**Figure 4J**). We then evaluated whether the skin cellular niches were remodeled by the AML cells as observed in their BM counterparts.[6] The proportion of Ebf2$^+$ MPCs in the skin stromal cells were reduced post-symptomatic onset of AML (**Figure 4K-4L**) whereas the Ebf2$^-$PαS cells remained unchanged (**Figure 4M-4N**). This finding is consistent with the reduced PαS cell fraction in the Ebf2$^+$ cells in AML mouse BM and might contribute to further AML cell proliferation since deletion of Ebf2$^+$ cells in mice led to AML acceleration.[6] In addition, while the total CD31$^+$ endothelial cells were unaltered, however, as observed in BM,[6] the CD31$^+$SCA1$^+$ arteriolar endothelial cells were significantly increased (**Figure 4O-4P**), indicating an increase of arterioles in dorsal skin during AML development.

Molecular evidence for the role of skin MPCs in hematopoiesis and AML

To investigate the molecular mechanisms behind the hematopoiesis-supportive function of the skin MPCs, we performed RNA sequencing on the freshly sorted skin Ebf2$^+$ and Ebf2$^-$PαS MPCs. This revealed a distinct transcriptional profile of skin MPCs and BM MSCs with 1150 and 816 genes differentially expressed between skin Ebf2$^+$ and Ebf2$^-$PαS MPCs compared to BM MSCs, respectively (**Figure 5A**). However, only 135 genes were differentially expressed between the skin Ebf2$^+$ and Ebf2$^-$PαS cells. Among them, the genes associated with TNFα signaling, angiogenesis and epithelial to mesenchymal transition, such as *Lama5* and *Tnc*, were upregulated while the cell proliferation genes were downregulated in the more primitive Ebf2$^+$ cells (**Figure 5B, Figure S5A**). We then compared skin MPC pool (Ebf2$^+$ and Ebf2$^-$PαS) with BM MSCs. The genes related to skin tissue maintenance (*Krt14*, *Krt19*) and adipogenesis (*Fabp4*) were upregulated in the skin MPCs (**Figure 5C**), showing tissue origin-related characteristics of these cells. Consistent with the limited chondrogenic differentiation capacity of skin MPCs (**Figure S1C-S1D**), the genes associated with osteogenesis and chondrogenesis were downregulated in the cells (**Figure S5B**). Conversely, skin MPCs were enriched with genes related to fatty acid metabolism and oxidative phosphorylation indicating a distinct metabolic profile between the skin and BM MSCs (**Figure 5D-5E**). Furthermore, the genes

related to inflammatory response were enriched in the skin MPCs relative to BM MSCs (**Figure 5E-5F, Figure S5C**), indicating a possible pro-inflammatory phenotype of skin MPCs.

Notably, no overall significant difference in the hematopoiesis supportive gene expression between the skin MPCs and BM MSCs (**Figure 5G**). The findings were confirmed by Q-PCR of the genes in these freshly sorted cells (**Figure 5H**). Similar to BM MSCs, both skin MPC subsets expressed *Cxcl12*, *Kitl* (*Scf*), *Jag1, Lama4* and *Angptl1,* all of which are known to be critical for hematopoiesis maintenance and regeneration.[37-44] The expressions of *Kitl*, *Jag1* and *Lama4* were even significantly higher in skin Ebf2^{+} and Ebf2^{-}PαS cells than that in BM MSCs. Moreover, the expression of *Spp1,* a negative regulator of HSC expansion,[45] was lower in skin MPCs than that in BM MSCs (**Figure 5C, 5H**).This finding support the similar function of skin MPCs and BM MSCs for HSCs and AML LSCs.

Enhanced mitochondrial transfer from skin MPCs to AML cells contributed to the chemoprotection of AML cells

To reveal the mechanisms underlying the function of skin MPCs in maintaining and protecting AML LSCs, we examined the metabolic support from skin MPCs to AML cells in coculture since the genes related to oxidative phosphorylation and fatty acid metabolism are enriched in the skin MPCs. Mitochondria transfer has been reported as one of the protective mechanisms during chemotherapy in leukemias to provide energy support and anti-oxidant machinery leading to modulating oxidative stress indued by chemotherapy[35,46-48]. In a co-culture with mitochondria-prelabeled skin MPCs (**Figure 6A**), we detected enhanced mitochondrial transfer from skin MPCs to the AML cells compared to BM MSCs (**Figure 6B-6C**). Correspondingly, the AML cells cocultured with skin MPCs showed lower ROS levels and higher viability during Ara-C treatment (**Figure 6D-6E**). These data indicated that skin MPCs could maintain AML LSCs and protect them from Ara-C treatment *in vitro* possibly by reducing oxidative stress. Thus, skin MPCs could be an important element in creating an extramedullary sanctuary for AML LSCs.

Lama4* loss in skin MPCs enhanced AML LSC proliferation and chemoprotection *in vitro

Lama4 was highly expressed in skin MPCs (**Figure 5H**) and we have found that *Lama4* loss in mice promoted AML LSC proliferation, chemoresistance, and relapse.[35] This has tempted us to test the impact of *Lama4* deletion in skin MPCs on AML LSC growth (**Figure 6F**). We observed increased AML cell proliferation and chemoresistance to Ara-C at 24h post-the co-

culture *Lama4*$^{-/-}$ skin MPCs (**Figure 6G**). Further CAFC assay indicated that *Lama4*$^{-/-}$ skin MPCs promoted AML LSC proliferation and chemoresistance to Ara-C (**Figure 6H**), suggesting a suppressive impact of *Lama4* expression in skin MPCs on AML cell growth and chemoresistance.

The increased chemoresistant AML cells in *Lama4*$^{-/-}$ mouse skin post-Ara-C treatment

To further explore the molecular mechanism involving in the role of the extramedullary niche in the skin for maintaining residual AML cells after chemotherapy, we here took advantage of *Lama4*$^{-/-}$ mice (**Figure 7A**) where AML progression and relapse are accelerated.[35] There was no homing preference of the AML cells to *Lama4*$^{-/-}$ skin and BM (**Figure S6**). One day post-Ara-C treatment, confocal imaging illustrated more residual AML cells retained in *Lama4*$^{-/-}$ mouse skin, compared to that in *Lama4*$^{+/+}$ mice following Ara-C treatment (**Figure 7B**). However, such a difference was not detected by FACS analysis while the elimination of the AML cells from the PB and skin were clearly observed (**Figure 7C**). It is possible that some of the remaining AML cells were lost during enzymatic digestion of the skin for FACS whereas confocal imaging was performed on the tissue fixed directly after dissecting. It is important to note that the chemoresistant CD36^{+} AML cells[15,33], not KIT^{+} cells were enriched in *Lama4*$^{-/-}$ mouse skin post-Ara-C treatment (**Figure 7D**), which was not observed in the BM, as reported.[35] These data suggest that *Lama4* expression in skin mesenchymal niche play a role in maintaining the chemosensitivity of AML cells in the skin to Ara-C.

Discussion

We here report that skin tissue harbored two distinct MPC subsets, the Ebf2^{+} and Ebf2^{-}PαS cells, sharing a similar phenotype with BM MSCs.[20,49,50] During AML development, similar to leukemia cutis observed in patients, a substantial amount of AML cells infiltrated in mouse skin. The AML cells were distributed along vascular sites and co-localized with the skin Ebf2^{+} cells. Importantly, these AML cells isolated from mice at steady-state and after chemotherapy could initiate AML post-transplantation into immunocompetent mice. Molecular characterization of the skin MPCs showed high expression of *Lama4*, *KitL* and *Jag1*, known to be important for normal hematopoiesis maintenance and leukemic cell proliferation.[31,35,37-44,51] The skin mesenchymal cell niche maintained AML LSCs and protected them from chemotherapeutic agent Ara-C. Furthermore, Lama4 loss in skin MPCs promoted AML proliferation and chemoresistance. Our study provides evidence for the characteristics and

previously unrecognized role of skin mesenchymal cell niche during AML development and after chemotherapy.

Leukemia cutis is commonly observed in monocytic AML (FAB, M5) and pediatric patients with congenital leukemia are prone to develop leukemia cutis, ranging from 25% to 30% of the cases.[52] It also correlates with manifestations of other extramedullary sites and is associated with a poor prognosis in patients.[1-3] However, leukemia cutis has been understudied. Its impact on AML relapse remains unexplored. We here show AML-regenerating capacity of the residual AML cells in skin post-chemotherapy, pointing to a possible involvement of these leukemic cells in the relapse of AML. In patients, leukemia cutis is usually present concurrently with AML cell infiltration in BM. However, in some cases, it may precede systemic involvement,[4] and it is unclear whether the leukemic cells infiltrated in the skin originate from BM.

We here for the first time show the chemoprotective role of skin MPCs for AML LSCs. Multiple mechanisms might be involved in the protection. Mitochondrial transfer from stromal cells to leukemic cells has been reported to be one of the mechanisms to protect leukemic cells to survive from chemotherapy by providing antioxidant system to counteract the therapy induced oxidative stress.[53] We here detected a mitochondrial transfer from skin MPCs to the AML cells during chemotherapy *in vitro,* even in a greater degree, than that from BM MSCs. This finding is in line with the enrichment of oxidative phosphorylation genes in skin MPCs. In addition, *Lama4* expression in skin MPCs seemed to maintain AML LSC chemosensitivity since *Lama4* loss in skin MPCs led to enhanced proliferation and chemoprotection of AML LSCs. In line with this, the residual chemoresistant $CD36^+$ AML cells in *Lama4*$^{-/-}$ skin were increased post-Ara-C treatment. Such an effect was not observed in the BM. One possible reason could be the differential expression *of Kitl*, *Jag1* and *Lama4*, known to be important for AML development.[31,35,54] Furthermore, the upregulated inflammatory genes in skin MPCs might have contributed to this effect.

Our findings of the identity and immunophenotype of skin MPCs will facilitate the prospective isolation of the cells for further characterization *ex vivo*. The skin $Ebf2^+$ MPCs co-express pericyte markers like CD140b/PDGFRb, NG2 and α-SMA and their perivascular location indicated their pericyte phenotype. A contribution of skin $Ebf2^+$ cells to mesenchymal cell turnover was illustrated by the *in vivo* lineage-tracing. The adjacent localization of the $Ebf2^+$ cells to the AML cells in skin indicated a possibility that these cells might act as a niche

component for maintaining AML cells. This notion was supported by another important finding showing a supportive function of skin MPCs for AML LSCs. The fractions skin Ebf2^{+} MPCs were reduced after symptomatic AML onset, leading to a reconstructed niche, which might in turn further promote AML progression since Ebf2^{+} cell deletion in mice accelerated AML development, as reported.[6]

In summary, we here report that skin harbors primitive Ebf2^{+} MPCs and the downstream Ebf2^{-} MPCs. These MPCs are colocalized with AML cells at perivascular sites during AML development. The residual AML cells in the skin after chemotherapy can regenerate leukemia post-transplantation, indicating the existence of AML LSCs in the skin. The skin MPCs can provide metabolic support for AML cells to protect them from chemotherapy *in vitro*. Loss of *Lama4* in skin MPCs further enhances their supportive and chemoprotective function for the leukemic cells. We for the first time provide evidence for the roles of skin mesenchymal cell niche for AML LSC growth and chemotherapy response, as well as the impact of *Lama4* expression on the niche protection or support. These findings warrant future studies on the role of skin mesenchymal niches in chemotherapy response and relapse of AML patients.

Methods

Mice

Ebf2-Egfp reporter FVB/N mice[22] at 8 to 14-week old were used. Transgenic *Ebf2-Egfp*X*Ebf2-Cre^{ERT2}*X *Rosa26^{loxp}Stop^{loxp}-Tomato* mice were generated by crossing *Ebf2-Egfp* with *Ebf2-Cre^{ERT2}*X*Rosa26^{loxp}Stop^{loxp}-Tomato* mice for lineage tracing. To activate Cre, tamoxifen (TAM) (Sigma) was intraperitoneally injected at 3mg/20g body weight for 3 times every second day.[6] *Lama4$^{-/-}$* C57BL/6 mice were generated as described.[55] All mice were maintained in specific-pathogen-free conditions in the animal facility of Karolinska Institute. Animal procedures were approved by local ethics committee (ethical number 1869) at Karolinska Institute (Stockholm, Sweden).

In vivo lineage tracing

This was performed as previously described.[6] Dorsal skin from triple transgenic *Ebf2-Egfp* x *Ebf2-Cre^{ERT2}* x *Rosa26^{loxp}Stop^{loxp}- Tomato* mice[6] were collected at 3, 6 and 12 months after tamoxifen injection. Approximately, 1x1cm of dorsal skin tissue was fixed and embedded in OCT for whole mount immunofluorescence. For evaluating the frequency of Ebf2^{+} cells and their progeny (Tomato^{+}), 2 x 2cm of dorsal skin tissue was processed for skin MPC isolation

by fluorescence-activated cell sorting (FACS) (BD FACS Aria™ III). For defining the gates for GFP$^+$ and Tomato$^+$ cells, cells from bi-transgenic or single transgenic mouse were used as fluorescence-minus one (FMO) controls. After excluding dead cells by propidium iodide (PI) staining, the CD45$^-$TER119$^-$CD31$^-$ stromal cells were gated. Subsequently, the CD44$^-$ fractions were divided based on CD140a and SCA1 expression.

Ara-C treatment and detection of residual AML cells *in vivo* was performed as described in the related study[35] .

Skin MPC isolation by FACS

Mouse dorsal skin was minced and digested with 0.2% collagenase II (CLSII Worthington Biochemicals) in PBS supplemented with 20% FBS for 60 minutes at 37°C. After washing with PBS/20%FBS followed by PBS, the digested skin tissue was treated with 0.05% trypsin-EDTA (GIBCO) for 10 to 15minutes at 37°C. Cell suspension was spun down at 300g for 10minutes. Mononuclear cells were then blocked with FcR (CD16/32) antibody and stained with CD45, TER119, CD31, CD44, CD140a, and SCA1 for 15minutes at 2-8°C. Dead cells were excluded by propidium iodide (PI) staining. For sorting native skin MPCs, hematopoietic and endothelial populations were firstly excluded (CD45$^-$TER119$^-$CD31$^-$) and Ebf2 gate was then defined based on Fluorescence Minus One (FMO) using skin mononuclear cells from a non-transgenic mouse. Skin Ebf2$^+$ and Ebf2$^-$ cells were sorted on a FACS Aria III Sorp (BD Biosciences, San Jose). See Table S1 for detailed antibody information.

Generation of MLL-AF9-induced AML mouse model

AML mouse model was induced as previously described.[6] Briefly, 250.000 MLL-AF9 expressing cells were intravenously injected into non-irradiated mice to generate the AML mouse model. For detecting AML infiltration in dorsal skin tissue, 1x10^6 of MLL-AF9 previously generated in DsRed C57BL/6J transgenic mice[56] were intravenously injected into sublethally irradiated (6Gy) *Lama4*$^{+/+}$ and *Lama4*$^{-/-}$ mice, as described[35]. At day 15, the mice were treated intraperitoneally with Cytarabine (Ara-C, Jena Bioscience) at the dose of 700mg/kg body weight, daily for 5 consecutive days. The mice were sacrificed one day after the last injection for AML engraftment analysis in peripheral blood (PB), BM and dorsal skin by FACS. The distribution of residual AML cells in dorsal skin was visualized by confocal imaging.

Serial transplantation

To test the leukemia-initiating capacity of the AML cells infiltrated in skin tissue, the AML CD45.1^{+} cells were sorted from skin tissue of the mice that have developed AML post-AML cell injection. The mice were treated with normal saline or Ara-C for 5 days at day 20-21 after AML cell injection. The AML cells in skin were collected 2-3days after the last injection, sorted by FACS and transplanted into non-irradiated secondary C57BL/6J recipient mice via tail vein at a dose of 1000 or 5000 cells per mouse. The AML development was monitored by blood analysis using FACS and Sysmex as well as by assessing the general health conditions. The survival rate of the mice was estimated based on the date when the mice were found dead or in moribund status. Bones and blood were collected for determining AML engraftment.

Multilineage differentiation assay

This was done as described [6]. The skin Ebf2^{+}, Ebf2^{-} and Ebf2^{-}PαS cells were expanded in culture and plated at 400cells / cm^{2} to each well of 24-well plate. For osteogenic differentiation, cells were cultured with complete osteogenic medium mixed by human/mouse StemXVivo osteogenic / adipogenic base medium (CCM007, R&D Systems) and mouse StemXVivo ostegenic supplement (CCM009; R&D Systems) under normoxic condition for 14-21 days. Differentiation toward osteoblast was evaluated by 1% alizarin red S (Catalog no A5533, Sigma) staining after cell fixation with cold methanol. For adipogenic differentiation, the culture was performed with DMEM containing 10% FBS, 10mM HEPES (1M), 100U of penicillin/streptomycin, 10^{-4} M 2-Mercaptoethanol (Sigma, catalog no.M7522), 5µg/mL insulin (Catalog no I6634, Sigma), 20µM Indomethacin (Catalog no I7378, Sigma), 0.0115 mg/mL isobutylmethylxanthine (Catalog no I-7018, Sigma), and 10^{-6} M dexamethasone (Catalog no D2915, Sigma) for 2-3 weeks. Cells were then fixed with 10% formalin and stained with 0.5% Oil Red O (Catalog no O1391, Sigma). Chondrogenic differentiation was induced in monolayer culture where cells were cultured with DMEM high glucose containing 10mM HEPES (1M), 100U of penicillin / streptomycin, 10^{-4} M 2-Mercaptoethanol (catalog no.M7522, Sigma), 2mM pyruvate (Catalog no P5280, Sigma), 0.35mM L-proline (Catalog no P5607-25G, Sigma), ITS^{+3} (Catalog no I-3146, Sigma), 5µg/mL L-ascorbic acid 2-phosphate (Catalog no A7506, Sigma), 10^{-7} M dexamethasone (Catalog No D2915, Sigma), and 10ng/mL TGF-β3 (Catalog no 100-36E, Peprotech). To assess chondrogenic differentiation, toluidine blue (Catalog no T3260, Sigma) (pH 2.0 to 2.5) was used to stain proteoglycan. Images were then taken under inverted microscope (CKX41, Olympus).

459

460 ***In vitro* chondrogenic induction in micromass pellet**

461 After *in vitro* expansion, 2.5x10^5 of BM MSCs or skin Ebf2$^+$ or skin Ebf2$^-$PαS MPCs were
462 collected in 15mL tube and spun down at 300g for 7 minutes. After removal of supernatant,
463 500 µM of chondrogenic medium consisting of DMEM high glucose with 10 mM HEPES,
464 100U of penicillin/streptomycin, 10^{-4} M 2-Mercaptoethanol (catalog no.M7522, Sigma), 2 mM
465 pyruvate (Catalog no P5280, Sigma), 0.35 mM L-proline (Catalog no. P5607-25G, Sigma),
466 ITS^{+3} (Catalog no. I-3146, Sigma), 5µg/mL L-ascorbic acid 2-phosphate (Catalog no. A7506,
467 Sigma), 10^{-7}M dexamethasone (Catalog No. D2915, Sigma,), and 10ng/mL TGF-β3 (Catalog
468 no. 100-36E, Peprotech) were added. The chondrogenic induction was performed in 37°C
469 under hypoxic condition (2% O_2). Every 2-3 days, the medium was replaced until day 28. For
470 evaluating the chondrogenic induction, the micromass pellets were washed with PBS prior
471 being fixed in 4% PFA for 2 days. After dehydration with 70% ethanol, the pellets were stained
472 with toluidine blue (Catalog no. T3260, Sigma) at pH 2.0 to 2.5 for 15–30 minutes. Thereafter,
473 the stained pellets were washed with 70% ethanol and embedded in OCT-compound (Catalog
474 no. 4583, Sakura Tissue Tex®,). To visualize the formation of proteoglycan, the embedded
475 pellet was cut to 10µm, mounted and observed by inverted microscope (Axio Observer.Z1,
476 Zeis). Images were processed with Zen software (Carl Zeiss Microscopy, GmbH 2011).

477

478 **Skin MPC expansion and proliferation kinetics *in vitro***

479 For *in vitro* expansion, CFU-Fs from FACS-sorted skin Ebf2$^+$ and Ebf2$^-$PαS cells were
480 trypsinized with 0.05% trypsin-EDTA (GIBCO), collected, and plated to T-25 flasks at 400
481 cells /cm^2. Cells were then expanded in complete Dulbecco modified Eagle Medium (DMEM,
482 catalog no.31966, GIBCO) containing 10% FBS, 10 mM HEPES (1M), 100U of penicillin /
483 streptomycin, and 10^{-4}M 2-Mercaptoethanol (catalog no.M7522, Sigma) under hypoxic
484 condition (1-2% O_2) until 80%-90% confluence was reached. Proliferation rates of skin Ebf2$^+$
485 and Ebf2$^-$PαS cells were evaluated by population doubling time (PDT) assays. PDT was
486 calculated by dividing number of days for culturing the cells with number of population
487 doublings (PDs) using following formula: PDT= Culture time (days)/PD where PD=log
488 (NH/NI)/ log 2, NH is harvested cell number and NI is initial cell number.

489

490 **Dorsal skin wholemount immunofluorescence staining**

Dorsal skin specimens were fixed in 4% PFA for 10 minutes followed by washing with PBS prior embedding in OCT-Compound (Sakura Tissue Tex®, Catalog no. 4583). For immunofluorescence staining, 150 µM dorsal skin sections were first blocked with skim milk, fish skin gelatin (Catalog no. G7765, Sigma) and Triton X-100 (Catalog no. T8787, Sigma) for 1hour at RT. To visualize Ebf2$^+$ cells in mouse dorsal skin, the sections were incubated with anti-GFP, additionally stained with either anti-mouse MECA32, CD31, NG2, NESTIN, or α-SMA antibodies. All stainings were performed at 2-8°C overnight prior washing with PBS and staining with secondary antibody. Imaging was performed with confocal microscopy at Live Cell Imaging (LCI) facility after the section was mounted in Mountant PermaFlour (Catalog no. TA-030-F19, Thermo). See Table S2 for antibodies used for the confocal imaging. Quantification of the Ebf2$^+$ or Ebf2/GFP$^-$Tomato$^+$ cells expressing NESTIN, NG2 or α-SMA was performed with NIS-element AR-analysis ver 5.20.00 64-bit software (Nikon). From 100µM section, 30-40µM thickness was scanned with a confocal microscope to localize Ebf2$^+$ and Ebf2$^+$ progenies (Ebf2/GFP$^-$Tomato$^+$ cells). Areas where Ebf2$^+$ and Ebf2/GFP$^-$Tomato$^+$ cells were distributed were further imaged every 1-1.1µM depth to obtain Region of interest (ROI). Within ROI, positive expression of NESTIN, NG2 or α-SMA was defined based on control sections stained with secondary antibodies only while GFP$^+$ signal was set based on samples from non-GFP reporter mice. Three to 4 mice were included for the quantification.

RNA sequencing

Total RNA from freshly sorted skin Ebf2$^+$ cells, skin Ebf2$^-$ PαS cells and BM MSCs were isolated with RNeasy Micro Kit (Qiagen) according to the manufacturer's protocol. cDNA was prepared using SMART-Seq v4 Ultra Low Input RNA Kit for Sequencing (Cat. No. 634898, Takara Bio.). The cDNA quality was examined on Agilent TapeStation system using a High Sensitivity D5000 ScreenTape (Cat. No. 5067-5592, Agilent). One ng cDNA was used for library preparation using *Nextera XT* DNA Library Preparation Kit (Cat. Nos. FC-131-1024 & FC-131-1096, Illumina). The yield and quality of the amplified libraries were analyzed using Qubit by Thermo Fisher and the Agilent Tapestation System. The indexed cDNA libraries were sequenced on the Illumina 2000 or Nextseq 550 (Illumina, San Diego, CA) for a 75-cycle v2 sequencing run generating 75 bp single-end reads. About 7-20 million reads/sample were obtained. Sample quality was assessed using FastQC (v0.11.8) and MultiQC (v1.7). Reads were aligned to a reference built from Ensembl GRCm38 genome sequences using STAR (v2.6.1d). All mapped counts to each gene were further calculated by FeatureCounts function

from Subread package [57] installed in R. Genes with Reads Per Kilobase of transcript per Million mapped reads (RPKM) values more than 0.1 were considered as being actively transcribed and proceeded to the analysis of Differential Gene Expression (DGE).[58] The normalized read counts assigned to each sample were generated by Deseq2. The differentially expressed genes between the cell subsets were identified by adjusted *P* value (*p*adj < 0.05) using Benjamini-Hochberg correction for multiple testing, together with thresholds at log_2fold changes >1 (up-regulated) or <-1 (down-regulated). For the Gene Set Enrichment Analysis (GSEA), the normalized read counts were imported into the GSEA (v4.0.3) platform from Broad Institute (http://www.broadinstitute.org/gsea/index.jsp), with three gene sets being tested, including gene ontology (c5.all.v5.symbols.gmt), hallmark (h.all.v5.symbols.gmt) and KEGG (c2.kegg.v5.symbols.gmt). Gene sets tested were considered to be statistically enriched when the nominal P value < .01 and FDR < .25.

LIN$^-$SCA1$^+$KIT$^+$ (LSK) CD150$^+$ cell isolation

Mouse femurs, tibia and iliac crest were crushed and washed with PBS/5% FBS to obtain BM mononuclear cells. Hematopoietic lineage (LIN) markers TER119, B220, GR-1, CD3, CD11b were firstly depleted with the use of sheep anti-rat DynaI beads (Invitrogen). LIN-depleted cells were then stained with anti-SCA1, anti-KIT, anti-CD150 and PECY5-conjugated antibodies against the LIN markers mentioned above. After excluding dead cells based on propidium iodiode (PI) staining, the LSKCD150$^+$ HSCs were sorted on BD FACS Aria III (BD Biosciences, San Jose) using DIVA 7.0 software. The gating was defined based on fluorescence minus one (FMO). See table S1 for antibody detail information.

Co-culture of skin MPCs with LSKCD150$^+$ cells and colony-forming cell in culture (CFU-C) assay

Twenty-five thousand (25,000) expanded Ebf2$^+$ or Ebf2$^-$PαS MPCs from skin and BM at passage 4-13 were plated into each well of 12-well plate and maintained in complete Dulbecco modified Eagle Medium (DMEM, catalog no.31966, GIBCO) containing 10% FBS, 10 mM HEPES (1M), 100U of penicillin/streptomycin and 10^{-4}M 2-Mercaptoethanol (catalog no.M7522, Sigma) under hypoxic condition (2% O_2) for 24h prior co-culture. The co-cultures were started by plating 2000 sorted LSKCD150$^+$ to each well in Myelocult medium (M5300, Stem Cell Technologies) supplemented with 10^{-6} M hydrocortisone (Catalog no 74142, Stem Cell Technologies,) and 1% penicillin streptomycin. After a 3-day co-culture in 5% CO_2 at

37°C, the medium containing hematopoietic cells and trypsinized cells were collected for FACS analysis and CFU-C assay in Methylcellulose M3434 (Stem Cell Technologies). After 10 days of culture at 37°C in 5% CO_2, CFU-Cs in the methylcellulose were stained with 2,7-diaminofluorene (DAF staining) and scored with an inverted microscope (CKX41, Olympus). A cell cluster with a minimum of 50 cells is defined as one colony. Colonies with positive DAF staining were defined as erythrocytes-containing colonies including CFU-GME and BFU-E), as performed previously.[9 59]

Cobblestone area-forming cells (CAFC) assay using primary skin MPCs

This was done as previously described.[60] Briefly, 30.000 skin or BM Ebf2$^+$ or Ebf2$^-$PαS MPCs were first plated into a 24-multiwell plate and maintained in complete Dulbecco modified Eagle Medium (DMEM, catalog no.31966, GIBCO) containing 10% FBS, 10mM HEPES (1M), 100U of penicillin/streptomycin, and 10^{-4}M 2-Mercaptoethanol (catalog no.M7522,Sigma) under hypoxic condition (1% O_2). One day after, 150-300 MLL-AF9 or LSK cells were then added on the MSCs and MPCs in Myelocult (M5300, Stem Cell Technologies) with 10^{-6} M hydrocortisone (Catalog no. 07904, Stem Cell Technologies,), 1% penicillin streptomycin and 1ng/mL IL-3 (R&D). The co-cultures were performed at 32°C in 5% CO_2 for 7-14 days. A CAFC was defined as a cluster of more than 3 cells underneath the MSCs/MPCs. The CAFCs were visualized and scored with inverted microscope (CKX41, Olympus) on day 7 and 10. At day 10-14, the cells were trypsinized and collected for FACS analysis of the KIT$^+$ and CD36$^+$ AML LSCs and their cell cycle status.

Detection of reactive oxygen species (ROS) level

The MSCs/MPCs or AML cells were harvested and washed with PBS and incubated with 2µM of H_2-DCFDA (C6827, ThermoFisher) in DMEM at 37°C for 40min to detect ROS level. The cells were then rinsed twice with PBS and resuspended with 150µL of Propidium iodide (1:1000) in 5%FBS/PBS. ROS levels were measured by FACS.

Mitochondrial transfer

MSCs or MPCs were stained with 100nM MitoTracker™ red FM (M22426, ThermoFisher) at 37°C for 60 min, according to the manufacturer's instructions. The cells were washed twice with PBS, then incubated for 3-4 hours to remove unbound probe before a final wash. Subsequently, 15,000-25,000 MLL-AF9 AML cells in Myelocult (M5300, StemCell

Technologies) were plated and cocultured with prelabelled MSCs for 24 hours. Mitochondrial transfer was quantified in AML cells ($CD45.1^+$) by FACS and analyzed for MFI of the mitoTracker red.

Colony-forming unit-fibroblast (CFU-F), RNA sequencing and **quantitative RT-PCR (Q-PCR)** were done as described.[6,35] See Table S3 for information of Assays-on-Demand probes.

Statistical analysis

Unless mentioned, either unpaired t-test or Mann-Whitney test was used to determine the difference between the groups or cell subsets. All statistical tests were performed with GraphPad Prism 8 software with $P < 0.05$ considered statistically significant.

Data availability

The RNA sequencing data are available at GEO under accession number GSE167562.

Acknowledgements

We thank Tina Jacob, Karl Annusver and Alexandra Are at Department of Cell and Molecular Biology, Karolinska Institute, Sweden for valuable advice and technical discussion. We thank Alexandre Piccini, Yuanyuan Zhang and Andranik Durguryan in our group for technical help for the cell culture. We also thank Prof. Marja Ekblom, Lund University for her scientific input. This study was supported by the Swedish Research Council (2019-01361), Swedish Childhood Cancer Society (PR2015-0142, FoAss13/015, PR2017/0154, PR2020-0166), Swedish Cancer Society (CAN2017/774, 19 0092 SIA and 20 1222PjF), Åke Olsson foundation, Radiumhemmets Forskningsfonder (151241, 171162, 191253) and Karolinska Institute Wallenberg Institute for Regenerative Medicine, Karolinska Institute doctoral education (KID) funding (2-1293/2014) to support LS, Stiftelsen Clas Groschinskys Minnesfond (ref:M16 50) to H.Q., and the Swedish Research Council (2018-02963) and Swedish Cancer Society (CAN 2018/793) to MK. FACS analysis and cell sorting were performed at MedH Flow Cytometry core facility (Karolinska Institute), supported by KI/SLL. The confocal images were obtained at the LCI facility/Nikon Center of Excellence, Karolinska Institute, supported by grants from the Knut and Alice Wallenberg Foundation, the Swedish Research Council, KI infrastructure,

623 Centre for Innovative Medicine and Jonasson center at the Royal Institute of Technology. All
624 major computations were performed on resources provided by the Swedish National
625 Infrastructure for Computing (SNIC) through Uppsala Multidisciplinary Center for Advanced
626 Computational Science (UPPMAX) under Project sens2018540. We also would like to thank
627 the core facility at NEO, BEA, Bioinformatics and Expression Analysis, which is supported by
628 the board of research at the Karolinska Institute and the research committee at the Karolinska
629 Hospital.

630

631 **Author contributions**

632 LS has substantially participated in designing, performing experiments, collecting and
633 analyzing data and manuscript writing. HC, PX, MK(Kondo), XS, EL and ASJ performed
634 experiments, collected data and assisted with data analysis and manuscript-editing. MK
635 (Kasper) provided scientific input and assistance with confocal imaging of skin tissues. MJ
636 provided the DsRed-expressing MLL-AF9 AML cells and scientific input on the manuscript.
637 KT provided Lama4$^{-/-}$ mouse models and scientific input. HQ designed, performed experiments,
638 collected and analyzed data, wrote the manuscript. All authors have proved the final version of
639 the manuscript.

640 **Conflict of interest:** All authors declare no competing financial interest regarding this study.

641

642 **References**

643

644 1 Bakst, R. L., Tallman, M. S., Douer, D. & Yahalom, J. How I treat extramedullary
645 acute myeloid leukemia. *Blood* **118**, 3785-3793, doi:10.1182/blood-2011-04-
646 347229 (2011).
647 2 Gouache, E. *et al.* Leukemia Cutis in Childhood Acute Myeloid Leukemia:
648 Epidemiological, Clinical, Biological, and Prognostic Characteristics of Patients
649 Included in the ELAM02 Study. *Hemasphere* **2**, e141,
650 doi:10.1097/HS9.0000000000000141 (2018).
651 3 Wang, C. X., Pusic, I. & Anadkat, M. J. Association of Leukemia Cutis With Survival
652 in Acute Myeloid Leukemia. *JAMA Dermatol* **155**, 826-832,
653 doi:10.1001/jamadermatol.2019.0052 (2019).
654 4 Krooks, J. A. & Weatherall, A. G. Leukemia cutis in acute myeloid leukemia signifies
655 a poor prognosis. *Cutis* **102**, 266;271;272 (2018).

5 Hoggatt, J., Kfoury, Y. & Scadden, D. T. Hematopoietic Stem Cell Niche in Health and Disease. *Annual review of pathology* **11**, 555-581, doi:10.1146/annurev-pathol-012615-044414 (2016).

6 Xiao, P. *et al.* Distinct roles of mesenchymal stem and progenitor cells during the development of acute myeloid leukemia in mice. *Blood advances* **2**, 1480-1494, doi:10.1182/bloodadvances.2017013870 (2018).

7 Raaijmakers, M. H. *et al.* Bone progenitor dysfunction induces myelodysplasia and secondary leukaemia. *Nature* **464**, 852-857, doi:nature08851 [pii]
10.1038/nature08851 (2010).

8 Dong, L. *et al.* Leukaemogenic effects of Ptpn11 activating mutations in the stem cell microenvironment. *Nature* **539**, 304-308, doi:10.1038/nature20131 (2016).

9 Xiao, P. *et al.* Sipa1 deficiency-induced bone marrow niche alterations lead to the initiation of myeloproliferative neoplasm. *Blood advances* **2**, 534-548, doi:10.1182/bloodadvances.2017013599 (2018).

10 Hanoun, M. *et al.* Acute myelogenous leukemia-induced sympathetic neuropathy promotes malignancy in an altered hematopoietic stem cell niche. *Cell stem cell* **15**, 365-375, doi:10.1016/j.stem.2014.06.020 (2014).

11 Schepers, K. *et al.* Myeloproliferative neoplasia remodels the endosteal bone marrow niche into a self-reinforcing leukemic niche. *Cell Stem Cell* **13**, 285-299, doi:10.1016/j.stem.2013.06.009 (2013).

12 Kim, J. A. *et al.* Microenvironmental remodeling as a parameter and prognostic factor of heterogeneous leukemogenesis in acute myeloid leukemia. *Cancer Res*, doi:10.1158/0008-5472.CAN-14-3379 (2015).

13 Jeong, S. Y., Kim, J. A. & Oh, I. H. The Adaptive Remodeling of Stem Cell Niche in Stimulated Bone Marrow Counteracts the Leukemic Niche. *Stem Cells*, doi:10.1002/stem.2870 (2018).

14 Han, J. *et al.* Adipose tissue is an extramedullary reservoir for functional hematopoietic stem and progenitor cells. *Blood* **115**, 957-964, doi:10.1182/blood-2009-05-219923 (2010).

15 Ye, H. *et al.* Leukemic Stem Cells Evade Chemotherapy by Metabolic Adaptation to an Adipose Tissue Niche. *Cell Stem Cell* **19**, 23-37, doi:10.1016/j.stem.2016.06.001 (2016).

16 Toma, J. G. *et al.* Isolation of multipotent adult stem cells from the dermis of mammalian skin. *Nat Cell Biol* **3**, 778-784, doi:Doi 10.1038/Ncb0901-778 (2001).

17 Kimlin, L. & Virador, V. Cellular populations isolated from newborn mouse skin including mesenchymal stem cells. *Methods in molecular biology* **989**, 217-233, doi:10.1007/978-1-62703-330-5_17 (2013).

18 Viswanathan, S. *et al.* Mesenchymal stem versus stromal cells: International Society for Cell & Gene Therapy (ISCT(R)) Mesenchymal Stromal Cell committee position statement on nomenclature. *Cytotherapy* **21**, 1019-1024, doi:10.1016/j.jcyt.2019.08.002 (2019).

19 Vaculik, C. *et al.* Human dermis harbors distinct mesenchymal stromal cell subsets. *J Invest Dermatol* **132**, 563-574, doi:10.1038/jid.2011.355 (2012).

20 Morikawa, S. *et al.* Prospective identification, isolation, and systemic transplantation of multipotent mesenchymal stem cells in murine bone marrow. *J Exp Med* **206**, 2483-2496, doi:jem.20091046 [pii]
10.1084/jem.20091046 (2009).

21 Pinho, S. *et al.* PDGFRalpha and CD51 mark human Nestin+ sphere-forming mesenchymal stem cells capable of hematopoietic progenitor cell expansion. *J Exp Med* **210**, 1351-1367, doi:10.1084/jem.20122252 (2013).

22 Qian, H. *et al.* Molecular characterization of prospectively isolated multipotent mesenchymal progenitors provides new insight into the cellular identity of mesenchymal stem cells in mouse bone marrow. *Molecular and cellular biology* **33**, 661-677, doi:10.1128/MCB.01287-12 (2013).

23 Armulik, A., Genove, G. & Betsholtz, C. Pericytes: developmental, physiological, and pathological perspectives, problems, and promises. *Developmental cell* **21**, 193-215, doi:10.1016/j.devcel.2011.07.001 (2011).

24 Kusumbe, A. P. *et al.* Age-dependent modulation of vascular niches for haematopoietic stem cells. *Nature* **532**, 380-384, doi:10.1038/nature17638 (2016).

25 Baryawno, N. *et al.* A Cellular Taxonomy of the Bone Marrow Stroma in Homeostasis and Leukemia. *Cell* **177**, 1915-1932 e1916, doi:10.1016/j.cell.2019.04.040 (2019).

26 Alonso, S. *et al.* Human bone marrow niche chemoprotection mediated by cytochrome P450 enzymes. *Oncotarget* **6**, 14905-14912 (2015).

27 Jin, L. *et al.* CXCR4 up-regulation by imatinib induces chronic myelogenous leukemia (CML) cell migration to bone marrow stroma and promotes survival of quiescent CML cells. *Mol Cancer Ther* **7**, 48-58, doi:10.1158/1535-7163.MCT-07-0042 (2008).

28 Iwamoto, S., Mihara, K., Downing, J. R., Pui, C. H. & Campana, D. Mesenchymal cells regulate the response of acute lymphoblastic leukemia cells to asparaginase. *J Clin Invest* **117**, 1049-1057, doi:10.1172/JCI30235 (2007).

29 Zhang, B. *et al.* Microenvironmental protection of CML stem and progenitor cells from tyrosine kinase inhibitors through N-cadherin and Wnt-beta-catenin signaling. *Blood* **121**, 1824-1838, doi:10.1182/blood-2012-02-412890 (2013).

30 Xu, X. *et al.* BM microenvironmental protection of CML cells from imatinib through Stat5/NF-kappaB signaling and reversal by Wogonin. *Oncotarget* **7**, 24436-24454, doi:10.18632/oncotarget.8332 (2016).

31 Somervaille, T. C. & Cleary, M. L. Identification and characterization of leukemia stem cells in murine MLL-AF9 acute myeloid leukemia. *Cancer Cell* **10**, 257-268, doi:10.1016/j.ccr.2006.08.020 (2006).

32 Landberg, N. *et al.* CD36 defines primitive chronic myeloid leukemia cells less responsive to imatinib but vulnerable to antibody-based therapeutic targeting. *Haematologica* **103**, 447-455, doi:10.3324/haematol.2017.169946 (2018).

33 Farge, T. *et al.* Chemotherapy-Resistant Human Acute Myeloid Leukemia Cells Are Not Enriched for Leukemic Stem Cells but Require Oxidative Metabolism. *Cancer discovery* **7**, 716-735, doi:10.1158/2159-8290.CD-16-0441 (2017).

34 Duarte, D. *et al.* Inhibition of Endosteal Vascular Niche Remodeling Rescues Hematopoietic Stem Cell Loss in AML. *Cell Stem Cell* **22**, 64-77 e66, doi:10.1016/j.stem.2017.11.006 (2018).

35 Cai, H. *et al.* Critical Role of Lama4 for Hematopoiesis Regeneration and Acute Myeloid Leukemia Progression. *Blood*, doi:10.1182/blood.2021011510 (2021).

36 Ahsberg, J. *et al.* Progression of progenitor B-cell leukemia is associated with alterations of the bone marrow micro-environment. *Haematologica* **105**, e102-e106, doi:10.3324/haematol.2018.214031 (2020).

37 Poulos, M. G. *et al.* Endothelial Jagged-1 is necessary for homeostatic and regenerative hematopoiesis. *Cell reports* **4**, 1022-1034, doi:10.1016/j.celrep.2013.07.048 (2013).

38 Calvi, L. M. *et al.* Osteoblastic cells regulate the haematopoietic stem cell niche. *Nature* **425**, 841-846 (2003).

39 Greenbaum, A. *et al.* CXCL12 in early mesenchymal progenitors is required for haematopoietic stem-cell maintenance. *Nature* **495**, 227-230, doi:10.1038/nature11926 (2013).

40 Omatsu, Y. *et al.* The essential functions of adipo-osteogenic progenitors as the hematopoietic stem and progenitor cell niche. *Immunity* **33**, 387-399, doi:10.1016/j.immuni.2010.08.017 (2010).

41 Arai, F. *et al.* Tie2/angiopoietin-1 signaling regulates hematopoietic stem cell quiescence in the bone marrow niche. *Cell* **118**, 149-161 (2004).

42 Thoren, L. A. *et al.* Kit regulates maintenance of quiescent hematopoietic stem cells. *J Immunol* **180**, 2045-2053 (2008).

43 Gu, Y. C. *et al.* Laminin isoform-specific promotion of adhesion and migration of human bone marrow progenitor cells. *Blood* **101**, 877-885 (2003).

44 Susek, K. H. *et al.* Bone marrow laminins influence hematopoietic stem and progenitor cell cycling and homing to the bone marrow. *Matrix Biol* **67**, 47-62, doi:10.1016/j.matbio.2018.01.007 (2018).

45 Stier, S. *et al.* Osteopontin is a hematopoietic stem cell niche component that negatively regulates stem cell pool size. *J Exp Med* **201**, 1781-1791 (2005).

46 Batsivari, A. *et al.* Dynamic responses of the haematopoietic stem cell niche to diverse stresses. *Nat Cell Biol* **22**, 7-17, doi:10.1038/s41556-019-0444-9 (2020).

47 Moschoi, R. *et al.* Protective mitochondrial transfer from bone marrow stromal cells to acute myeloid leukemic cells during chemotherapy. *Blood* **128**, 253-264, doi:10.1182/blood-2015-07-655860 (2016).

48 Marlein, C. R. *et al.* NADPH oxidase-2 derived superoxide drives mitochondrial transfer from bone marrow stromal cells to leukemic blasts. *Blood* **130**, 1649-1660, doi:10.1182/blood-2017-03-772939 (2017).

49 Qian, H., Le Blanc, K. & Sigvardsson, M. Primary mesenchymal stem and progenitor cells from bone marrow lack expression of CD44 protein. *The Journal of biological chemistry* **287**, 25795-25807, doi:10.1074/jbc.M112.339622 (2012).

50 Qian, H. *et al.* Molecular characterization of prospectively isolated multipotent mesenchymal progenitors provides new insight into the cellular identity of mesenchymal stem cells in mouse bone marrow. *Mol Cell Biol* **33**, 661-677, doi:10.1128/MCB.01287-12 (2013).

51 Wang, W. *et al.* Aberrant Notch Signaling in the Bone Marrow Microenvironment of Acute Lymphoid Leukemia Suppresses Osteoblast-Mediated Support of Hematopoietic Niche Function. *Cancer Res* **76**, 1641-1652, doi:10.1158/0008-5472.CAN-15-2092 (2016).

52 Parsi, M., Go, M. S. & Ahmed, A. in *StatPearls* (2020).

53 Forte, D. *et al.* Bone Marrow Mesenchymal Stem Cells Support Acute Myeloid Leukemia Bioenergetics and Enhance Antioxidant Defense and Escape from Chemotherapy. *Cell Metab*, doi:10.1016/j.cmet.2020.09.001 (2020).

54 Kode, A. *et al.* FoxO1-dependent induction of acute myeloid leukemia by osteoblasts in mice. *Leukemia* **30**, 1-13, doi:10.1038/leu.2015.161 (2016).

55 Thyboll, J. *et al.* Deletion of the laminin alpha4 chain leads to impaired microvessel maturation. *Mol Cell Biol* **22**, 1194-1202 (2002).

56 Hartwell, K. A. *et al.* Niche-based screening identifies small-molecule inhibitors of leukemia stem cells. *Nat Chem Biol* **9**, 840-848, doi:10.1038/nchembio.1367 (2013).

57 Liao, Y., Smyth, G. K. & Shi, W. The Subread aligner: fast, accurate and scalable read mapping by seed-and-vote. *Nucleic acids research* **41**, e108, doi:10.1093/nar/gkt214 (2013).

58 Mortazavi, A., Williams, B. A., McCue, K., Schaeffer, L. & Wold, B. Mapping and quantifying mammalian transcriptomes by RNA-Seq. *Nat Methods* **5**, 621-628, doi:10.1038/nmeth.1226 (2008).

59 McGuckin, C. P., Forraz, N. & Liu, W. M. Diaminofluorene stain detects erythroid differentiation in immature haemopoietic cells treated with EPO, IL-3, SCF, TGFbeta1, MIP-1alpha and IFNgamma. *European journal of haematology* **70**, 106-114 (2003).

60 van Os, R. P., Dethmers-Ausema, B. & de Haan, G. In vitro assays for cobblestone area-forming cells, LTC-IC, and CFU-C. *Methods Mol Biol* **430**, 143-157, doi:10.1007/978-1-59745-182-6_10 (2008).

Figure Legends

Figure 1 AML cells infiltrated in skin are capable to regenerate AML post-transplantation

(**A**) Strategy to generate MLL-AF9 AML mouse model. MLL-AF9 transduced AML cells expressing CD45.1 were transplanted into non-irradiated CD45.2 C57BL/6 mice.

(**B**) FACS profile showing AML engraftment analysis in BM, peripheral blood (PB) and dorsal skin at the end stage of AML. The numbers in the panel are the mean frequencies.

(**C**) Proportion of the AML cells within total hematopoietic ($CD45^+$) cell in dorsal skin and PB. Data were from 6 independent experiments and each dot represents data from a mouse. The horizontal bars represent mean values. Paired t-test was used for statistical analysis.

(**D**) Distribution of MLL-$AF9^+$ AML cells expressing DsRed at perivascular sites in dorsal skin. The endothelial cells were marked by CD31 expression (white).

(**E**) Experimental strategy to test AML-initiating capacity of the AML cells infiltrated in mouse skin by serial transplantation. The primary recipient mice (CD45.2) that developed AML post-AML cell (CD45.1) transplantation were treated with Ara-C or saline (NS, untreated). The residual $CD45.1^+$ AML cells from skin were sorted at 2-3days after the last injection of Ara-C and transplanted into secondary non-irradiated CD45.2 C57BL/6 mice at doses of 1000 (1K)-5000 (5K) cells/mouse, respectively. The AML development was monitored by FACS and hematology analyzer Sysmex. The mice were sacrificed when found dead or moribund.

(**F**) The Kaplan-Meier survival curve of the secondary recipient mice which received skin-derived AML cells sorted from primary recipients after treatment with Ara-C or normal saline. The date was the time when the mice were found dead or moribund. The survival curve was generated by Log-rank (Mantel-Cox test).

(**G**) Platelet counts in PB of the secondary recipient mice at the endpoint.

(**H**) FACS profile showing the engraftment of skin-derived AML CD45.1$^+$ cells in BM of the secondary recipient mice.

(**I**) The engraftment levels of the skin-derived AML CD45.1$^+$ cells in BM of the secondary recipient mice.

(**J**) Spleen size of the recipient mice at the endpoint.

(**K**) The frequencies of the secondary mice that developed AML after injection of skin-derived AML cells.

Figure 2 Identification of skin MPC subsets by Ebf2 expression.

(**A**) A representative FACS profile showing FACS sorting/analysis of the Ebf2$^+$ and Ebf2$^-$ cells in dorsal skin. The cells were first gated within non-hematopoietic (CD45$^-$TER119$^-$) and non-endothelial (CD31$^-$) live (PI$^-$) stromal cells. Then, these cells lacking expression of CD44 were further analyzed for their expression of SCA1, PDGFRa/CD140a (PαS) and CD51. The numbers in the panel are the mean frequencies.

(**B-C**) The Ebf2$^+$ cell frequency within total PI$^-$ (**B**) or PI$^-$CD45$^-$TER119$^-$CD31$^-$ stromal cells (**C**) in dorsal skin.

(**D**) The fractions of PαS cells within the Ebf2$^+$ and Ebf2$^-$ stromal cells. Each dot in **B-D** represents data from a single mouse in 3-6 experiments with the horizontal line as a mean value.

(**E**) CFU-Fs in the Ebf2$^+$ and Ebf2$^-$ stromal cells.

(**F**) CFU-Fs were exclusively found in the Ebf2$^+$SCA1$^+$ cell fraction. Data in **E-F** are from 3 independent experiments and each dot represents replicate assays from 2-3 mice in each experiment. The horizontal line represents mean value. Wilcoxon matched-signed pair rank test was used for statistical analysis.

(G-J) Single-cell analysis of CFU-Fs and lineage differentiation from the FACS-sorted Ebf2$^+$ (**G-H**) and Ebf2$^-$PαS (**I-J**) stromal cells. The CFU-F frequencies (**G**, **I**) were determined by limiting dilution at a density of 1, 2, 5, 10 cells per well in a 96-well plate and the frequency of the single cells with bi-lineage plasticity (**H, J**) were assessed by multilineage differentiation potential of single CFU-Fs derived from the cells.

(**K**) Representative images of the osteogenic and adipogenic differentiation from single CFU-F clones derived from Ebf2$^+$ and Ebf2$^-$PαS cells.

(**L**) Population-doubling time (PDT) of randomly selected CFU-Fs derived from single Ebf2$^+$ and Ebf2$^-$PαS cells. Each line represents the growth kinetics of a single clone.

See also in Figure S1.

Figure 3 Distribution and hierarchical relationship of skin MPCs.

(**A**) Localization of Ebf2$^+$ cells in skin perivascular area (Box 1) and in dermal panniculus carnosus (DPC). The endothelial cells in the vessels were identified by MECA32 staining.

(**B**) Representative image showing the perivascular localization of Ebf2$^+$ cells adjacent to CD31$^+$ endothelial cells in dorsal skin.

(**C**) A scheme showing strategy for lineage-tracing of the Ebf2$^+$ cells in skin. The Ebf2/GFP$^+$Tomato$^+$ cells and their progenies (Ebf2/GFP$^-$Tomato$^+$) were traced by FACS at 3, 6, 12 months after tamoxifen injection.

(**D**) A representative FACS profile showing analysis of activated Ebf2$^+$ cells (GFP$^+$Tomato$^+$) and their progeny (GFP$^-$Tomato$^+$). The gates for different cell subsets were defined with FMO from bi-transgenic or single transgenic mice. Each stromal cell subset (PI$^-$CD45$^-$TER119$^-$CD31$^-$) was gated within the CD44$^-$ fractions and subsequently gated for PαS cells based on CD140a and SCA1 expression.

(**E**) The frequencies of Ebf2/GFP$^+$Tomato$^+$ cells and its progenies (Ebf2/GFP$^-$Tomato$^+$) within stromal cells.

(**F**) The fractions of PαS and Ebf2$^-$CD140a$^+$SCA1$^-$ cells within total GFP$^-$Tomato$^+$ cells generated by Ebf2$^+$ cells. Each dot represents data from each mouse from 2-3 independent experiments. Horizontal bars represent the mean., and unpaired *t*-test were used for statistical analysis.

(**G**) Distribution of the single Ebf2/GFP$^+$Tomato$^-$ cells (green), activated Ebf2/GFP$^+$Tomato$^+$ cells (orange) and Ebf2/GFP$^-$Tomato$^+$ (red) cells at 3 months after tamoxifen injection.

See also in Figure S2-S3.

Figure 4 Skin MPCs support AML LSC growth and protect them from chemotherapy.

(**A**) Experimental strategy for assessing the role of the skin MPC and BM MSC subsets for AML growth by cobblestone area-forming cell (CAFC) assay.

(**B**) Representative images of CAFCs derived from the AML cells.

(**C**) Total numbers of CAFCs generated from 150 MLL-AF9$^+$ AML cells.

(**D**) A proportion of residual CAFCs from AML cells after Ara-C treatment relative to the normal saline (NS)-treated controls.

(**E**) The total number of the AML cells at 10 days after Ara-C treatment.

(**F-G**) The frequency (F) and the numbers (G) of the KIT$^+$ AML LSCs.

(**H-I**) The frequency (H) and the numbers (I) of the CD36$^+$ chemoresistant AML cells.

Data in C-I were from 3-4 independent experiments and each dot represents the mean of replicate assays. The horizontal bars represent mean values. Unpaired (C-E, G, I) or paired (F,H) *t*-test was used for statistical analysis.

(**J**) Co-localization of AML cells (red) with the Ebf2$^+$ cells. Ebf2 was determined by GFP (green) and the endothelial cells were marked by CD31 (white).

(**K**) Representative FACS plot showing analysis of Ebf2$^+$ MPCs in AML mouse dorsal skin.

(**L**) The frequency of the Ebf2$^+$ MPCs within stromal cells in dorsal skin tissue at endstage of AML. Data were from 6 independent experiments and each dot represents a mouse. The horizontal bars represent mean values. Unpaired t-test was used for statistical analysis.

(**M**) Representative FACS plot showing analysis of the skin Ebf2$^-$PαS MPCs in healthy controls and AML mice.

(**N**) The frequency of the Ebf2$^-$PαS cells within stromal cells in dorsal skin at the end stage of AML. Data were from 6 independent experiments and each dot represents a mouse. The horizontal bars represent mean values. Unpaired t-test or Mann-Whitney was used for statistical analysis.

(**O**) FACS profile showing analysis of CD31$^+$ cells in the dorsal skin of healthy and AML mice.

(**P**) The frequency of total endothelial cells (CD31$^+$) and arteriolar endothelial cells (CD31$^+$SCA1$^+$).

Figure 5 RNA sequencing revealed the molecular profile of skin Ebf2$^+$ and Ebf2$^-$PαS MPCs.

(**A**) Venn diagram showing differentially expressed genes (DEG) among the skin Ebf2$^+$ MPCs, skin Ebf2$^-$PαS MPCs and BM MSCs.

(**B**) Gene set enrichment analysis (GSEA) revealed the enrichment of genes associated with different biological processes and cellular responses in the skin Ebf2$^+$ and Ebf2$^-$PαS MPC subsets.

(**C**) A volcano plot showing differentially expressed genes between skin MPCs (Ebf2$^+$ and Ebf2$^-$PαS) and BM MSCs.

(**D**) GSEA revealed the enrichment of gene sets associated with various biological processes and cellular responses in the skin MPCs (Ebf2$^+$ and Ebf2$^-$PαS) and BM MSCs.

(**E**) GSEA plots showing the enrichment of genes related to oxidative phosphorylation, inflammatory and interferon alpha response in the skin MPCs compared to that in BM MSCs. FDR (false discovery rate) and *P* values are indicated in the panels.

(**F**) Heatmap showing the expressions of selected inflammatory cytokines in skin Ebf2$^+$ cells, Ebf2$^-$PαS cells and BM MSCs. The heatmap was created in Excel using conditional formatting. The color scale was set based on the minimum, midpoint and maximum values of each gene in each row. Red correlates with high expression and green correlates with low expression.

(**G**) Gene sets enrichment plot showing hematopoiesis supportive niche genes in skin MPC subsets and BM MSCs, and the heatmap showing the gene expression levels.

(**H**) Q-PCR of HSC niche genes in BM MSCs, skin Ebf2$^+$ and Ebf2$^-$PαS MPCs. Each dot represents mean of triplicate measurement of the gene expression relative to *Hprt*. Horizontal bars represent the mean values. Data were from 3 independent sorting experiments. Unpaired *t*-tests were used as statistical analysis.

See also in Figure S4.

Figure 6 Mitochondrial transfer and Lama4 deficiency in skin MPCs contributed to the chemoprotection of AML cells from Ara-C.

(**A**) Experimental strategy for determining mitochondrial transfer from stromal cells to AML cells *in vitro*. Skin MPCs and BM MSCs that were prelabelled with MitoTracker red were co-cultured with MLL-AF9$^+$ AML cells for 24 hours. Ara-C was added 4-6 hours after seeding the AML cells.

(**B**) Mean fluorescence intensity (MFI) of MitoTracker showing mitochondrial transfer from the stromal cells to AML cells in the cocultures. The AML cells were co-cultured with BM MSCs and skin PαS MPCs pre-labeled with MitoTracker red. The stromal cell-derived mitochondria were detected by MFI of MitoTracker in the AML cells at 24h post-coculture by FACS. Data shown are normalized MitoTracker MFI in the AML cells based on the values of that in the AML co-cultured with BM MSCs without Ara-C treatment. Each dot represents mean values of 3-4 replicated measurements in each experiment of 4. Horizontal bars are median values.

(**C**) Representative FACS histograms showing MitoTracker MFI in the AML cells 24h post coculture with the stromal cells. The MFI from AML cells in the monoculture without the prelabeled MPCs was used as a negative control.

(**D**) ROS levels in the AML cells cocultured with BM MSCs or skin PαS MPCs 24h post-Ara-C treatment. Each dot represents the average value of triplicate assays from each experiment of 3. Horizontal bars are mean values.

(**E**) The % of PI^- live AML cells in the cocultures 24h after Ara-C treatment. Each dot represents mean values of 3-4 replicated measurements in each experiment of 4. Horizontal bars are median values.

The statistical differences in (B-E) among different types of cultures were determined by unpaired *t* test, and between NS and Ara-C treated groups within the same type of co-cultures were analyzed by paired t test.

(**F**) Experimental layout for assessing the impact of *Lama4* loss in skin MPCs for AML growth *in vitro* using a co-culture system. The *Lama4*$^{+/+}$ and *Lama4*$^{-/-}$ skin MPCs were co-cultured with MLL-AF9 AML cells in a 96-well plate. For CAFC assay, Ara-C was added 2 days post-seeding of AML cells. The numbers of total AML cells and CAFCs were counted at 24-28h and day 7 post-seeding AML cells, respectively.

(**G**) Fold changes in the number of the AML cells in the co-cultures with *Lama4*$^{-/-}$ skin MPCs in relation to that with *Lama4*$^{+/+}$ MPCs 24hours after Ara-C or saline treatment. Data were from 4 independent experiments and each dot represents the mean of triplicate assays. The horizontal bars represent mean values. Paired *t*-test was used for statistical analysis.

(**H**) The number of CAFCs derived from AML cells in the co-cultures with *Lama4*$^{+/+}$ and *Lama4*$^{-/-}$ skin MPCs treated with NS or Ara-C. Data shown are triplicate values from 2-3 independent experiments. The horizontal bars represent mean values. Unpaired *t*-test was used for statistical analysis.

Figure 7 A high level of residual AML cell infiltration in skin tissue of AML-promoting *Lama4*$^{-/-}$ mouse model post Ara-C treatment.

(**A**) Experimental setup. *Lam4*$^{+/+}$ and *Lama4*$^{-/-}$ mice were treated with normal saline (NS) or Ara-C at day 15 after injection of DsRed-expressing MLL-AF9$^+$ AML cells. Peripheral blood (PB) and BM were collected for FACS and confocal microscopy at 1-day after NS or Ara-C treatment.

(**B**) Representative confocal images showing residual AML cells in dorsal skin at 1-day post-Ara-C treatment.

(**C**) Frequency of AML cells in PB and skin at 1-day post-Ara-C treatment.

(**D**) Proportion of $CD36^+$ and KIT^+ AML LSCs in skin at 1-day post-Ara-C treatment.

Data were from 2-5 experiments and each dot in C-D represents data from a single mouse. The horizontal bars represent the mean values. Unpaired *t*-test was used for statistical analysis.

See also in Figure S6.

Figure 1

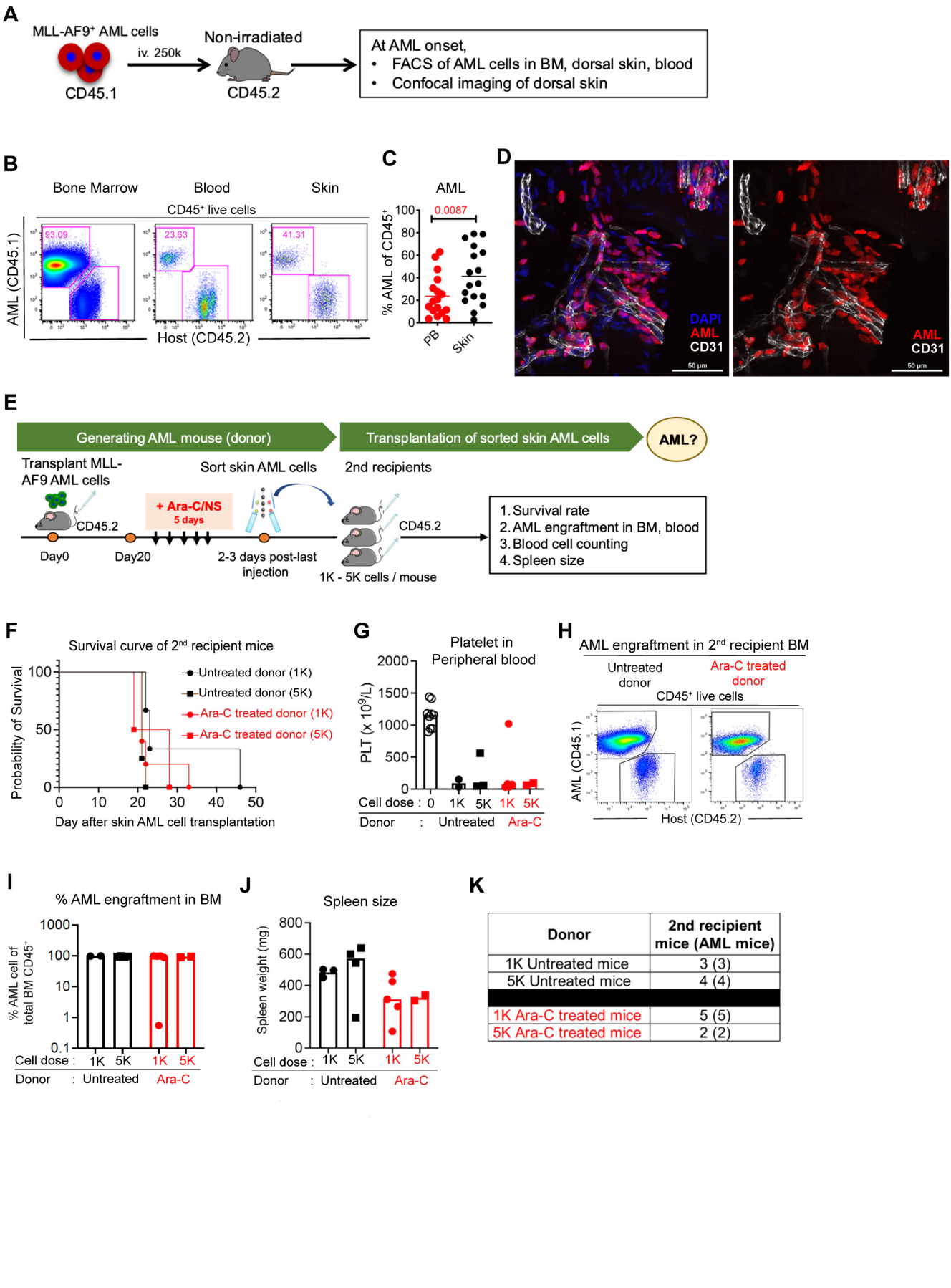

K

Donor	2nd recipient mice (AML mice)
1K Untreated mice	3 (3)
5K Untreated mice	4 (4)
1K Ara-C treated mice	5 (5)
5K Ara-C treated mice	2 (2)

Figure 2

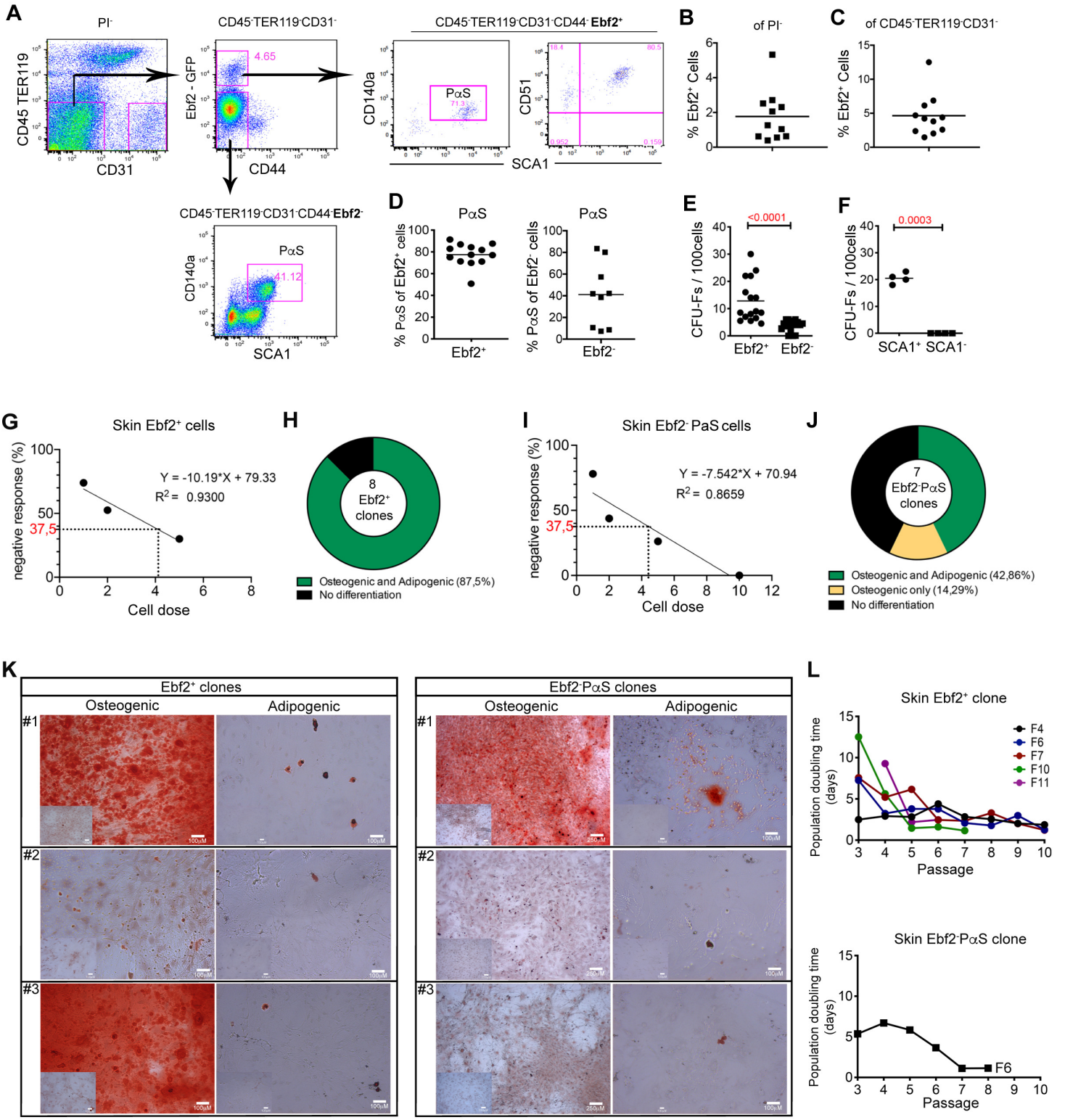
A
PI-
CD45-TER119-CD31-
CD45-TER119-CD31-CD44- Ebf2+
CD45 TER119
CD31
Ebf2 - GFP
4.65
CD44
CD140a
PαS
71.3
CD51
SCA1
18.4
80.5
0.952
0.159
CD45-TER119-CD31-CD44- Ebf2-
PαS
41.12
B
of PI-
% Ebf2+ Cells
C
of CD45-TER119-CD31-
% Ebf2+ Cells
D
PαS
% PαS of Ebf2+ cells
Ebf2+
PαS
% PαS of Ebf2- cells
Ebf2-
E
<0.0001
CFU-Fs / 100cells
Ebf2+
Ebf2-
F
0.0003
CFU-Fs / 100cells
SCA1+
SCA1-
G
Skin Ebf2+ cells
negative response (%)
Y = -10.19*X + 79.33
R2 = 0.9300
37,5
Cell dose
H
8
Ebf2+
clones
Osteogenic and Adipogenic (87,5%)
No differentiation
I
Skin Ebf2- PaS cells
negative response (%)
Y = -7.542*X + 70.94
R2 = 0.8659
37,5
Cell dose
J
7
Ebf2-PαS
clones
Osteogenic and Adipogenic (42,86%)
Osteogenic only (14,29%)
No differentiation
K
Ebf2+ clones
Osteogenic
Adipogenic
#1
#2
#3
Ebf2-PαS clones
Osteogenic
Adipogenic
#1
#2
#3
L
Skin Ebf2+ clone
Population doubling time (days)
Passage
F4
F6
F7
F10
F11
Skin Ebf2-PαS clone
Population doubling time (days)
Passage
F6

Figure 3

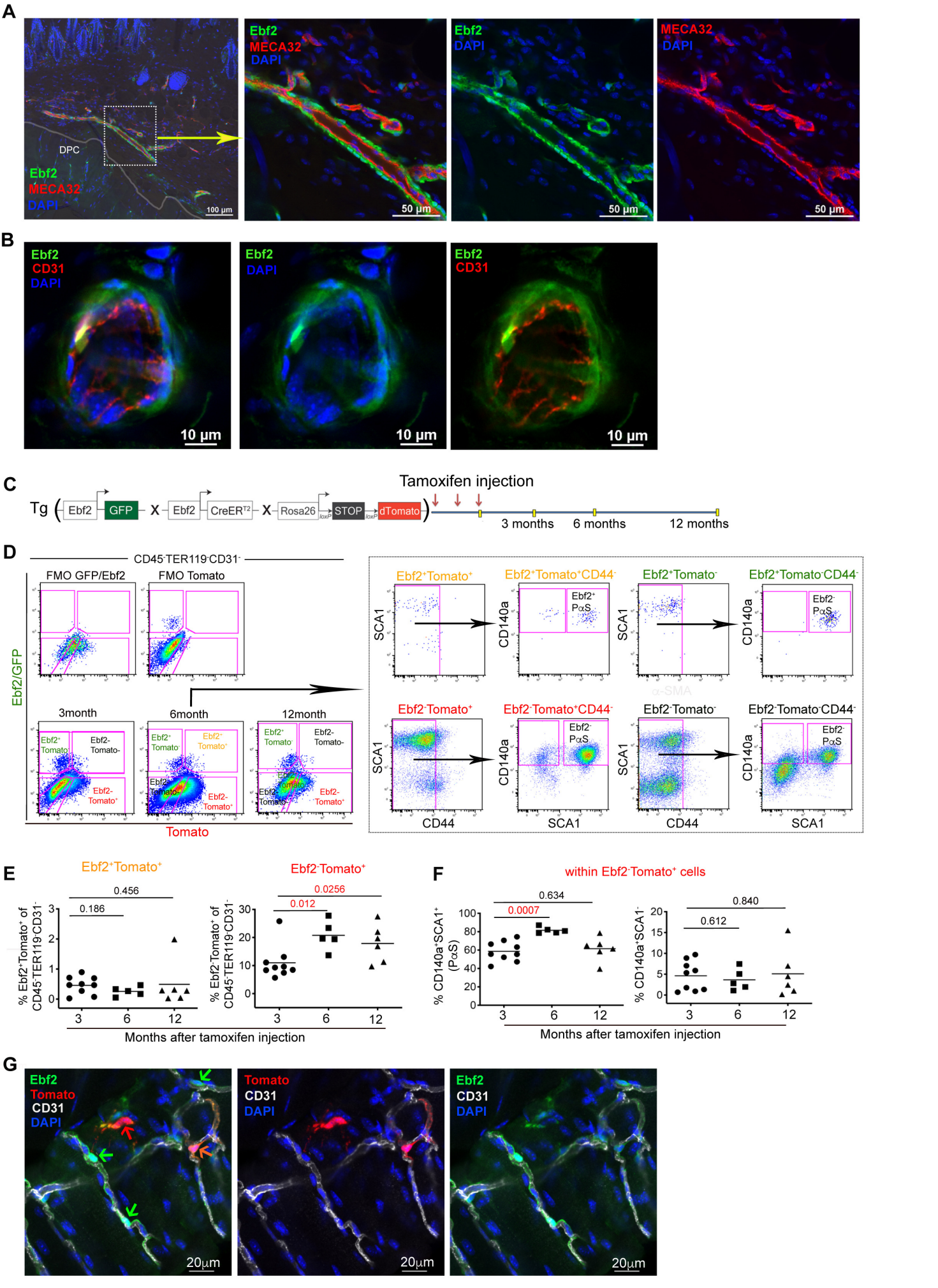
A
DPC
Ebf2
MECA32
DAPI
100 μm
Ebf2
MECA32
DAPI
50 μm
Ebf2
DAPI
50 μm
MECA32
DAPI
50 μm
B
Ebf2
CD31
DAPI
10 μm
Ebf2
DAPI
10 μm
Ebf2
CD31
10 μm
C
Tamoxifen injection
Tg
Ebf2
GFP
X
Ebf2
CreER^{T2}
X
Rosa26
loxP
STOP
loxP
dTomato
3 months
6 months
12 months
D
CD45$^-$TER119$^-$CD31$^-$
FMO GFP/Ebf2
FMO Tomato
Ebf2/GFP
3month
6month
12month
Ebf2$^+$ Tomato$^-$
Ebf2- Tomato-
Ebf2- Tomato$^+$
Tomato
Ebf2$^+$Tomato$^+$
Ebf2$^+$Tomato$^+$CD44$^-$
Ebf2$^+$Tomato$^-$
Ebf2$^+$Tomato$^-$CD44$^-$
Ebf2$^-$Tomato$^+$
Ebf2$^-$Tomato$^+$CD44$^-$
Ebf2$^-$Tomato$^-$
Ebf2$^-$Tomato$^-$CD44$^-$
SCA1
CD140a
CD44
Ebf2$^+$ PαS
Ebf2$^-$ PαS
α-SMA
E
Ebf2$^+$Tomato$^+$
Ebf2$^-$Tomato$^+$
0.456
0.186
0.0256
0.012
% Ebf2$^+$Tomato$^+$ of CD45$^-$TER119$^-$CD31$^-$
% Ebf2$^-$Tomato$^+$ of CD45$^-$TER119$^-$CD31$^-$
Months after tamoxifen injection
F
within Ebf2$^-$Tomato$^+$ cells
0.634
0.0007
0.840
0.612
% CD140a$^+$SCA1$^+$ (PαS)
% CD140a$^+$SCA1$^-$
Months after tamoxifen injection
G
Ebf2
Tomato
CD31
DAPI
20μm
Tomato
CD31
DAPI
20μm
Ebf2
CD31
DAPI
20μm

Figure 4

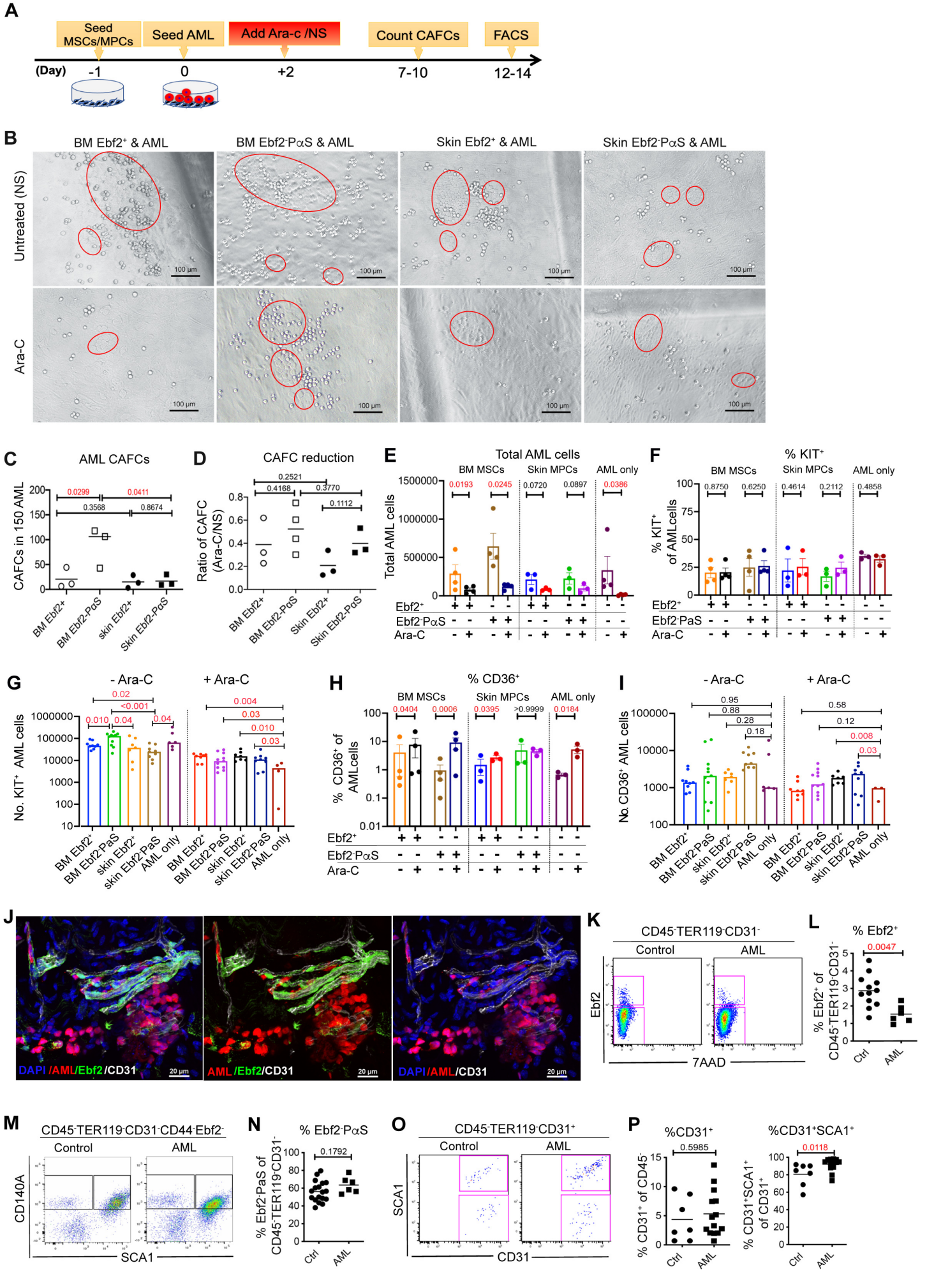
A
Seed MSCs/MPCs
Seed AML
Add Ara-c /NS
Count CAFCs
FACS
(Day)
-1
0
+2
7-10
12-14
B
BM Ebf2+ & AML
BM Ebf2-PαS & AML
Skin Ebf2+ & AML
Skin Ebf2-PαS & AML
Untreated (NS)
Ara-C
100 µm
C
AML CAFCs
CAFCs in 150 AML
0.0299
0.0411
0.3568
0.8674
BM Ebf2+
BM Ebf2-PαS
skin Ebf2+
Skin Ebf2-PαS
D
CAFC reduction
Ratio of CAFC (Ara-C/NS)
0.2521
0.4168
0.3770
0.1112
E
Total AML cells
BM MSCs
Skin MPCs
AML only
Total AML cells
0.0193
0.0245
0.0720
0.0897
0.0386
Ebf2+
Ebf2-PαS
Ara-C
F
% KIT+
BM MSCs
Skin MPCs
AML only
% KIT+ of AMLcells
0.8750
0.6250
0.4614
0.2112
0.4858
G
- Ara-C
+ Ara-C
No. KIT+ AML cells
0.02
<0.001
0.010
0.04
0.04
0.004
0.03
0.010
0.03
BM Ebf2+
BM Ebf2-PaS
skin Ebf2+
skin Ebf2-PaS
AML only
H
% CD36+
BM MSCs
Skin MPCs
AML only
% CD36+ of AMLcells
0.0404
0.0006
0.0395
>0.9999
0.0184
I
- Ara-C
+ Ara-C
No. CD36+ AML cells
0.95
0.88
0.28
0.18
0.58
0.12
0.008
0.03
J
DAPI /AML/Ebf2/CD31
AML/Ebf2/CD31
DAPI/AML/CD31
20 µm
K
CD45-TER119-CD31-
Control
AML
Ebf2
7AAD
L
% Ebf2+
% Ebf2+ of CD45-TER119-CD31-
0.0047
Ctrl
AML
M
CD45-TER119-CD31-CD44-Ebf2-
Control
AML
CD140A
SCA1
N
% Ebf2-PαS
% Ebf2-PaS of CD45-TER119-CD31-
0.1792
Ctrl
AML
O
CD45-TER119-CD31+
Control
AML
SCA1
CD31
P
%CD31+
% CD31+ of CD45-
0.5985
%CD31+SCA1+
% CD31+SCA1+ of CD31+
0.0118
Ctrl
AML

Figure 5

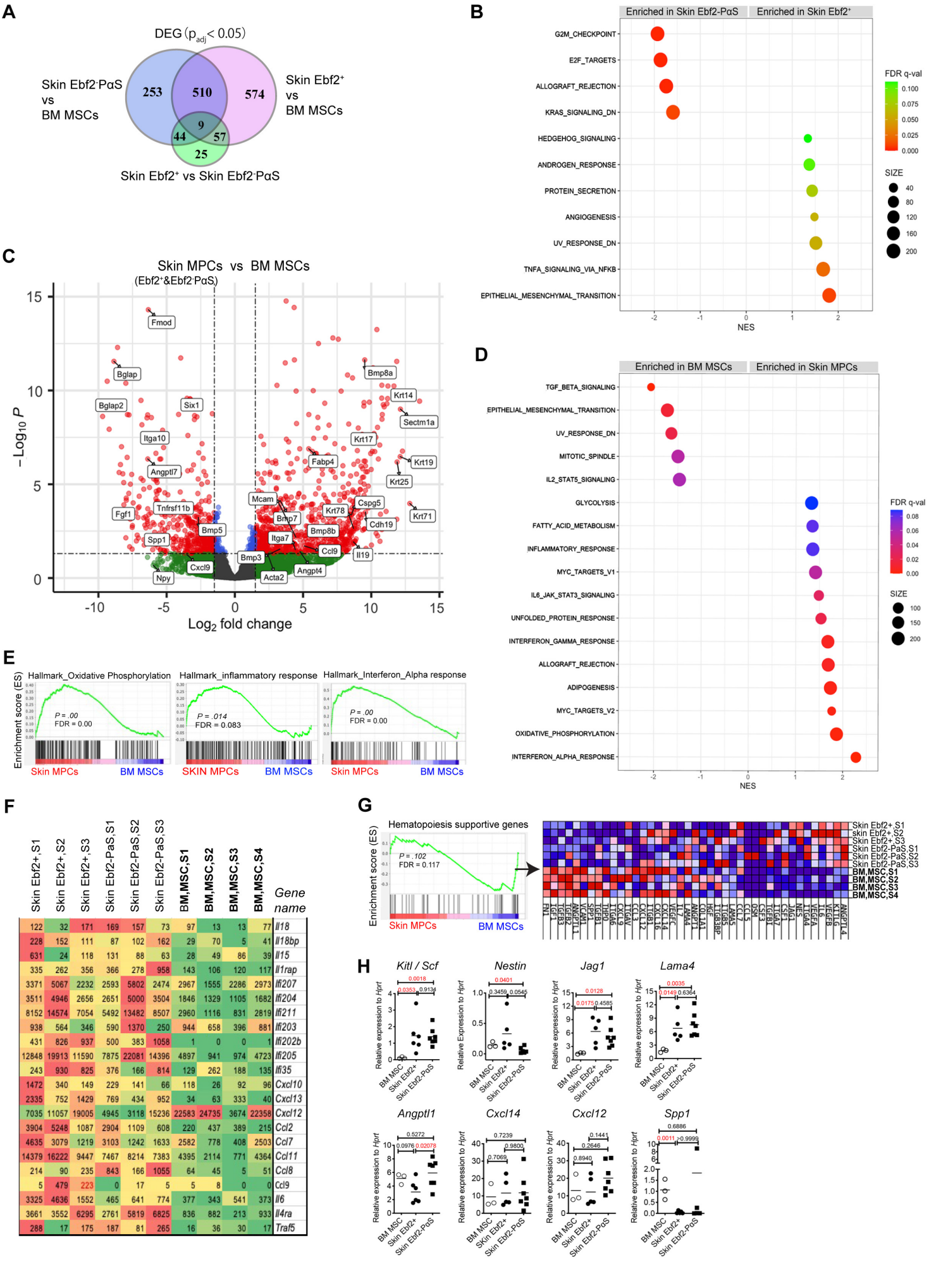
A
DEG (p_{adj} < 0.05)
Skin Ebf2-PαS vs BM MSCs
Skin Ebf2+ vs BM MSCs
Skin Ebf2+ vs Skin Ebf2-PαS
253
510
574
9
44
57
25
B
Enriched in Skin Ebf2-PαS
Enriched in Skin Ebf2+
G2M_CHECKPOINT
E2F_TARGETS
ALLOGRAFT_REJECTION
KRAS_SIGNALING_DN
HEDGEHOG_SIGNALING
ANDROGEN_RESPONSE
PROTEIN_SECRETION
ANGIOGENESIS
UV_RESPONSE_DN
TNFA_SIGNALING_VIA_NFKB
EPITHELIAL_MESENCHYMAL_TRANSITION
NES
FDR q-val
SIZE
C
Skin MPCs vs BM MSCs
(Ebf2+&Ebf2-PαS)
−Log10 P
Log2 fold change
Fmod
Bglap
Bglap2
Six1
Itga10
Angptl7
Fgf1
Tnfrsf11b
Spp1
Bmp5
Cxcl9
Npy
Bmp3
Acta2
Angpt4
Itga7
Bmp7
Mcam
Krt78
Bmp8b
Ccl9
Il19
Cdh19
Cspg5
Fabp4
Bmp8a
Krt14
Sectm1a
Krt17
Krt19
Krt25
Krt71
D
Enriched in BM MSCs
Enriched in Skin MPCs
TGF_BETA_SIGNALING
EPITHELIAL_MESENCHYMAL_TRANSITION
UV_RESPONSE_DN
MITOTIC_SPINDLE
IL2_STAT5_SIGNALING
GLYCOLYSIS
FATTY_ACID_METABOLISM
INFLAMMATORY_RESPONSE
MYC_TARGETS_V1
IL6_JAK_STAT3_SIGNALING
UNFOLDED_PROTEIN_RESPONSE
INTERFERON_GAMMA_RESPONSE
ALLOGRAFT_REJECTION
ADIPOGENESIS
MYC_TARGETS_V2
OXIDATIVE_PHOSPHORYLATION
INTERFERON_ALPHA_RESPONSE
NES
FDR q-val
SIZE
E
Enrichment score (ES)
Hallmark_Oxidative Phosphorylation
P = .00
FDR = 0.00
Skin MPCs
BM MSCs
Hallmark_inflammatory response
P = .014
FDR = 0.083
SKIN MPCs
BM MSCs
Hallmark_Interferon_Alpha response
P = .00
FDR = 0.00
Skin MPCs
BM MSCs
F
Skin Ebf2+,S1
Skin Ebf2+,S2
Skin Ebf2+,S3
Skin Ebf2-PaS,S1
Skin Ebf2-PaS,S2
Skin Ebf2-PaS,S3
BM,MSC,S1
BM,MSC,S2
BM,MSC,S3
BM,MSC,S4
Gene name
122 32 171 169 157 73 97 13 13 77 Il18
228 152 111 87 102 162 29 70 5 41 Il18bp
631 24 118 131 88 63 28 49 86 39 Il15
335 262 356 366 278 958 143 106 120 117 Il1rap
3371 5067 2232 2593 5802 2474 2967 1555 2286 2973 Ifi207
3511 4946 2656 2651 5000 3504 1846 1329 1105 1682 Ifi204
8152 14574 7054 5492 13482 8507 2960 1116 831 2819 Ifi211
938 564 346 590 1370 250 944 658 396 881 Ifi203
431 826 937 500 383 1058 1 0 0 1 Ifi202b
12848 19913 11590 7875 22081 14396 4897 941 974 4723 Ifi205
243 930 825 376 166 814 129 262 188 135 Ifi35
1472 340 149 229 141 66 118 26 92 96 Cxcl10
2335 752 1429 769 434 952 34 63 333 40 Cxcl13
7035 11057 19005 4945 3118 15236 22583 24735 3674 22358 Cxcl12
3904 5248 1087 2904 1109 608 220 437 389 215 Ccl2
4635 3079 1219 3103 1242 1633 2582 778 408 2503 Ccl7
14379 16222 9447 7467 8214 7383 4395 2114 771 4364 Ccl11
214 90 235 843 166 1055 64 45 5 51 Ccl8
5 479 223 0 17 5 5 8 0 0 Ccl9
3325 4636 1552 465 641 774 377 343 541 373 Il6
3661 3552 6295 2761 5819 6825 836 882 213 933 Il4ra
288 17 175 187 81 265 16 36 30 17 Traf5
G
Hematopoiesis supportive genes
Enrichment score (ES)
P = .102
FDR = 0.117
Skin MPCs
BM MSCs
Skin Ebf2+,S1
skin Ebf2+,S2
Skin Ebf2+,S3
Skin Ebf2-PaS,S1
Skin Ebf2-PaS,S2
Skin Ebf2-PaS,S3
BM,MSC,S1
BM,MSC,S2
BM,MSC,S3
BM,MSC,S4
FN1 TGFB3 TGFB2 ANGPT1 ANGPTL1 SPP1 VCAM1 TGFB1 TNPO TYRO3 ITGA6 ITGAV CCL3 CXCL12 CXCL16 ITGB1 VEGFC IL7 LAMA4 ANGPT1 COL1A1 HGF IGF1R ITGB5 LAMA5 CCL5 CCL7 OSM IL3 TGFB1 ITGA7 CSF1 JAG1 NES VEGFA IL6 VEGFB ANGPTL4 KITLG
H
Kitl / Scf
Nestin
Jag1
Lama4
Angptl1
Cxcl14
Cxcl12
Spp1
Relative expression to Hprt
BM MSC
Skin Ebf2+
Skin Ebf2-PaS

Figure 6

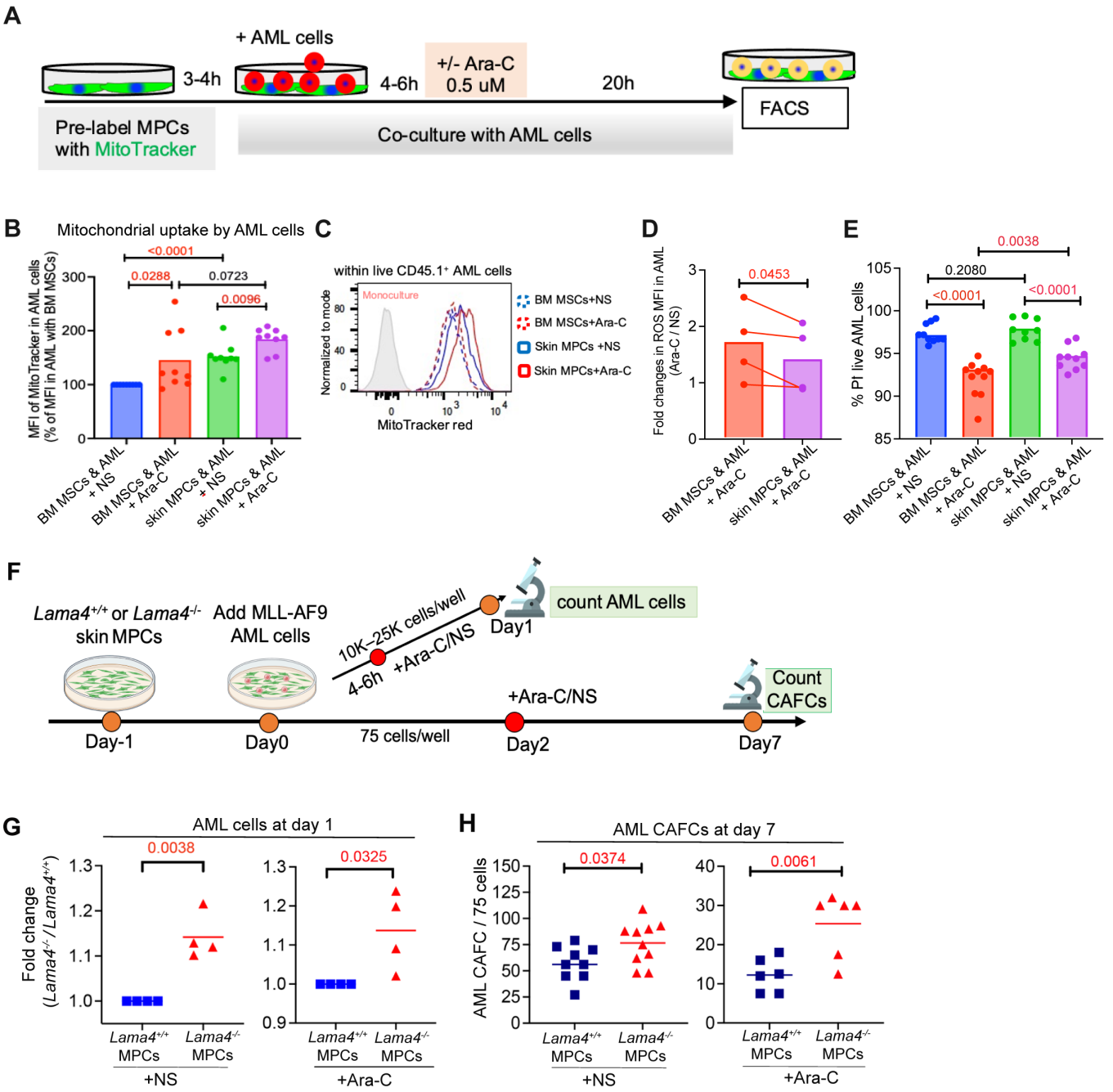
A
+ AML cells
3-4h
4-6h
+/- Ara-C
0.5 uM
20h
FACS
Pre-label MPCs
with MitoTracker
Co-culture with AML cells
B
Mitochondrial uptake by AML cells
MFI of MitoTracker in AML cells
(% of MFI in AML with BM MSCs)
<0.0001
0.0288
0.0723
0.0096
BM MSCs & AML + NS
BM MSCs & AML + Ara-C
skin MPCs & AML + NS
skin MPCs & AML + Ara-C
C
within live CD45.1+ AML cells
Monoculture
Normalized to mode
MitoTracker red
BM MSCs+NS
BM MSCs+Ara-C
Skin MPCs +NS
Skin MPCs+Ara-C
D
Fold changes in ROS MFI in AML
(Ara-C / NS)
0.0453
E
% PI live AML cells
0.0038
0.2080
<0.0001
<0.0001
F
Lama4+/+ or Lama4-/- skin MPCs
Add MLL-AF9 AML cells
10K–25K cells/well
4-6h
+Ara-C/NS
Day1
count AML cells
Day-1
Day0
75 cells/well
Day2
+Ara-C/NS
Count CAFCs
Day7
G
AML cells at day 1
Fold change
(Lama4-/- / Lama4+/+)
0.0038
0.0325
Lama4+/+ MPCs
Lama4-/- MPCs
+NS
+Ara-C
H
AML CAFCs at day 7
AML CAFC / 75 cells
0.0374
0.0061

Figure 7

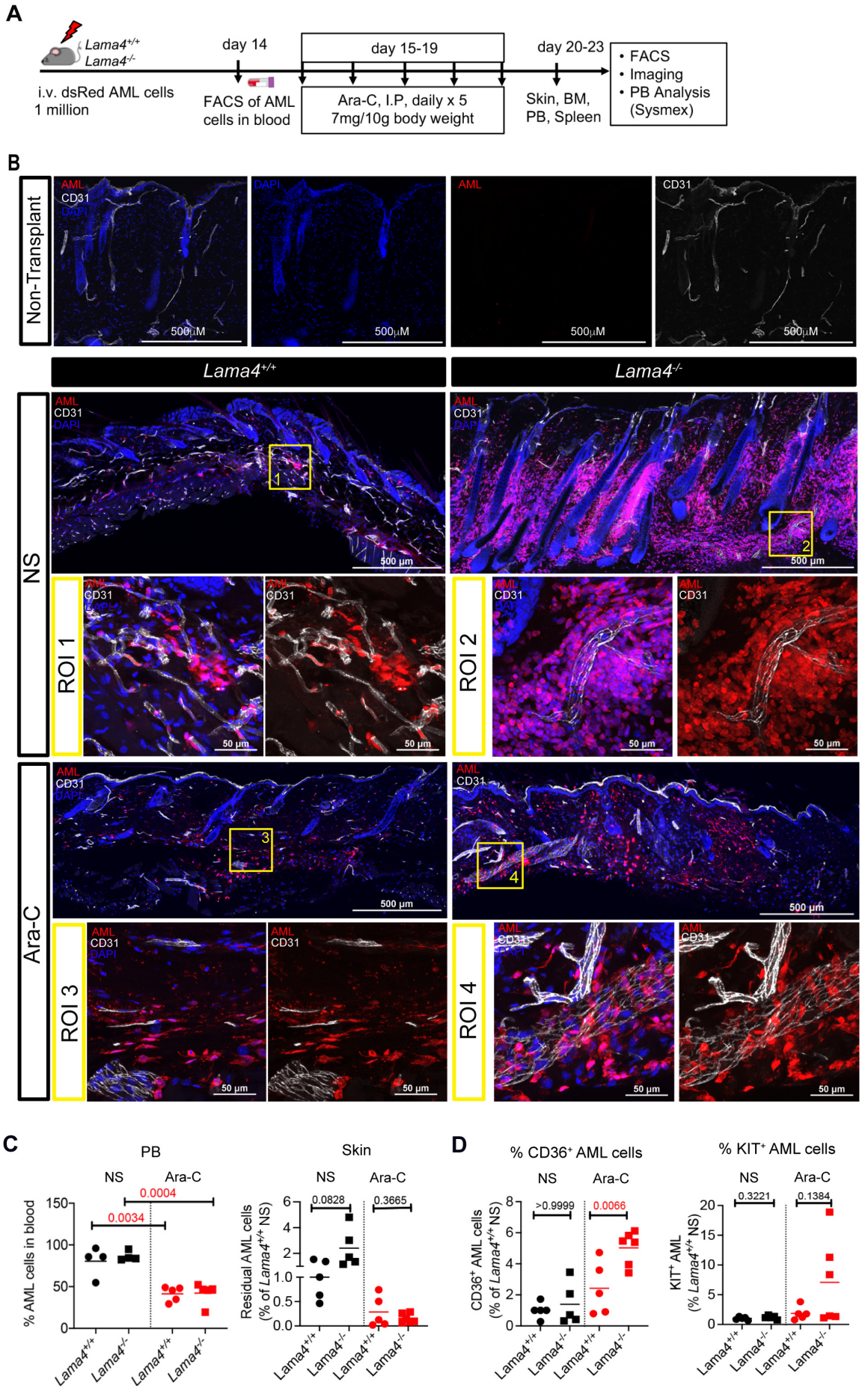
A
Lama4+/+
Lama4-/-
i.v. dsRed AML cells
1 million
day 14
FACS of AML
cells in blood
day 15-19
Ara-C, I.P, daily x 5
7mg/10g body weight
day 20-23
Skin, BM,
PB, Spleen
• FACS
• Imaging
• PB Analysis
(Sysmex)
B
Non-Transplant
AML
CD31
DAPI
500μM
Lama4+/+
Lama4-/-
NS
ROI 1
ROI 2
Ara-C
ROI 3
ROI 4
500 μm
50 μm
C
PB
Skin
NS
Ara-C
0.0004
0.0034
0.0828
0.3665
% AML cells in blood
Residual AML cells
(% of Lama4+/+ NS)
Lama4+/+
Lama4-/-
D
% CD36+ AML cells
% KIT+ AML cells
>0.9999
0.0066
0.3221
0.1384
CD36+ AML cells
(% of Lama4+/+ NS)
KIT+ AML
(% Lama4+/+ NS)